AGU PUBLICATIONS

Paleoceanography

RESEARCH ARTICLE
10.1002/2016PA003028

Key Points:
- Heinrich Layer 1 is represented by a double peak in the central North Atlantic
- Best estimates for the ages of the two peaks are ~16.1 (H1.1) and ~15 ka (H1.2)
- Heinrich Event 1 cannot account for cooling and weakened AMOC during early Heinrich Stadial 1 (~20–16.1 ka)

Supporting Information:
- Supporting Information S1
- Movie S1
- Movie S2
- Figure S1
- Figure S2
- Figure S3

Correspondence to:
D. A. Hodell,
dah73@cam.ac.uk

Citation:
Hodell, D. A., et al. (2017), Anatomy of Heinrich Layer 1 and its role in the last deglaciation, *Paleoceanography*, *32*, 284–303, doi:10.1002/2016PA003028.

Received 29 AUG 2016
Accepted 8 MAR 2017
Accepted article online 15 MAR 2017
Published online 30 MAR 2017

Anatomy of Heinrich Layer 1 and its role in the last deglaciation

David A. Hodell[1], Joseph A. Nicholl[1], Tomaso R. R. Bontognali[2], Steffan Danino[3], Javier Dorador[4], Julian A. Dowdeswell[3], Joshua Einsle[1], Holger Kuhlmann[5], Belen Martrat[6], Maryline J. Mleneck-Vautravers[1], Francisco Javier Rodríguez-Tovar[4], and Ursula Röhl[5]

[1]Godwin Laboratory for Palaeoclimate Research, Department of Earth Sciences, University of Cambridge, Cambridge, UK, [2]Geological Institute and Institute of Geochemistry and Petrology, ETH Zurich, Zurich, Switzerland, [3]Scott Polar Research Institute, Department of Geography, University of Cambridge, Cambridge, UK, [4]Departamento de Estratigrafía y Paleontología, Universidad de Granada, Granada, Spain, [5]MARUM–Center for Marine Environmental Sciences, University of Bremen, Bremen, Germany, [6]Department of Environmental Chemistry, Institute of Environmental Assessment and Water Research (IDÆA), Spanish Council for Scientific Research (CSIC), Barcelona, Spain

Abstract X-ray fluorescence (XRF) core scanning and X-ray computed tomography data were measured every 1 mm to study the structure of Heinrich Event 1 during the last deglaciation at International Ocean Discovery Program Site U1308. Heinrich Layer 1 comprises two distinct layers of ice-rafted detritus (IRD), which are rich in detrital carbonate (DC) and poor in foraminifera. Each DC layer consists of poorly sorted, coarse-grained clasts of IRD embedded in a dense, fine-grained matrix of glacial rock flour that is partially cemented. The radiocarbon ages of foraminifera at the base of the two layers indicate a difference of 1400 ^{14}C years, suggesting that they are two distinct events, but the calendar ages depend upon assumptions made for surface reservoir ages. The double peak indicates at least two distinct stages of discharge of the ice streams that drained the Laurentide Ice Sheet through Hudson Strait during HE1 or, alternatively, the discharge of two independent ice streams containing detrital carbonate. Heinrich Event 1.1 was the larger of the two events and began at ~16.2 ka (15.5–17.1 ka) when the polar North Atlantic was already cold and Atlantic Meridional Overturning Circulation (AMOC) weakened. The younger peak (H1.2) at ~15.1 ka (14.3 to 15.9 ka) was a weaker event than H1.1 that was accompanied by minor cooling. Our results support a complex history for Heinrich Stadial 1 (HS1) with reduction in AMOC during the early part (~20–16.2 ka) possibly driven by melting of European ice sheets, whereas the Laurentide Ice Sheet assumed a greater role during the latter half (~16.2–14.7 ka).

1. Introduction

Heinrich layers (HLs) in North Atlantic sediments are formed from massive discharges of the Hudson Strait ice stream that drained the Laurentide Ice Sheet [*Heinrich*, 1988; *Bond et al*., 1992; *Broecker et al*., 1992; *Hemming*, 2004]. These layers are identified in North Atlantic sediment cores by poorly sorted sediments that are almost devoid of foraminifera and contain large amounts of ice-rafted detritus (IRD), which is rich in detrital carbonate (DC) sourced from Paleozoic limestone and dolostone from the region of Hudson Bay and Hudson Strait [*Broecker et al*., 1992]. The layers are found from the Labrador Sea in the western Atlantic to off the coast of Portugal in the eastern North Atlantic along a zonal axis between 40 and 50°N in the so-called "Ruddiman IRD belt" [*Ruddiman*, 1977]. The deposits thin eastward from 40–70 cm in the Labrador Sea to <5 cm in the central North Atlantic, to <1 cm in the east [*Dowdeswell et al*., 1995].

Although Heinrich layers were first identified in the open North Atlantic [*Heinrich*, 1988], they have been correlated with detrital carbonate deposits from the Labrador Sea [*Andrews and Tedesco*, 1992; *Stoner et al*., 1996]. Deposits close to Hudson Strait show a more complete history of Heinrich layers but are affected by depositional processes other than ice rafting [*Hesse et al*., 2004; *Rashid et al*., 2012; *Hesse*, 2016]. The complexity of the deposits is related to the release of subglacial meltwater that entrains sediment, triggering the transport of fine material within nepheloid flows and turbidity currents [*Hesse and Khodabakhsh*, 1998, 2016; *Rashid et al*., 2003, 2012]. Such flows provide an additional mechanism for the delivery of detrital to the deep sea, resulting in several different types of deposits in the Labrador Sea [*Hesse*, 2016].

In distal deposits in the open North Atlantic, Heinrich layers consist mainly of IRD and are almost devoid of planktonic foraminifera [*Heinrich*, 1988; *Broecker et al*., 1992]. *Rashid et al*. [2003] suggested that distal

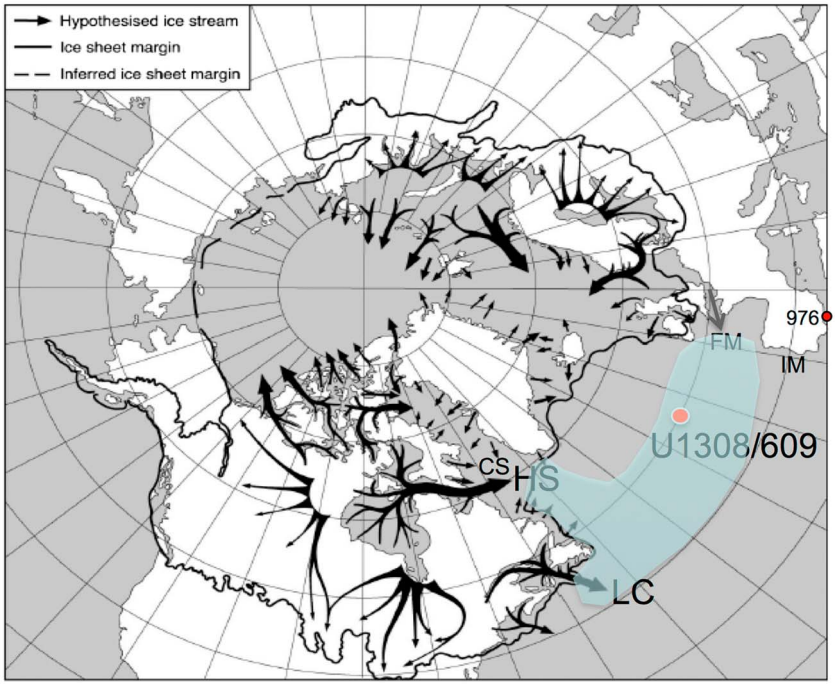

Figure 1. Location of Site U1308 in the IRD belt (blue shade) relative to reconstructed ice sheet extent in the Northern Hemisphere (continuous solid black line) showing the inferred locations of ice streams (black arrows; after *Denton and Hughes* [1981]) at the Last Glacial Maximum. HS = Hudson Strait; CS = Cumberland Sound; LC = Laurentian Channel; and FM = Fleuve Manche. Figure modified after *Stokes and Clark* [2001]. Also shown is the Iberian Margin (IM) and location of Site 976.

events are recorded as a single IRD layer that corresponds to only part of the sequence found in cores proximal to Hudson Strait. However, some detailed studies of distal HEs have suggested that the events may be more complex than a single episode of ice rafting. For example, a record of IRD from the Iberian Margin shows two distinct peaks in IRD during HE1 (i.e., H1a and H1b) [*Bard et al*., 2000], although only the older of these peaks contains DC (H1b). The younger H1a contains hematite-coated grains (3%) but almost no detrital carbonate. On the Laurentian Fan, *Gil et al*. [2015] identified two ice-rafting events during H1 that are associated with strong cooling and expansion of sea ice. Similar to the Iberian Margin, the older peak is rich in detrital carbonate and the younger is rich in hematite-stained grains.

Here we examined the detailed structure of Heinrich Stadial 1 at International Ocean Discovery Program (IODP) Site U1308 (49°52.6661′N; 24°14.2875′W) (Figure 1), which is located within the ice-rafted detritus (IRD) belt of the North Atlantic [*Ruddiman*, 1977]. Site U1308 represents the reoccupation of DSDP Site 609, which has played an important role in the recognition of Heinrich events and correlation of millennial-scale climate variability between marine sediment and Greenland ice cores [*Broecker et al*., 1992; *Bond et al*., 1992, 1993, 1999; *McManus et al*., 1994; *Bond and Lotti*, 1995].

Site U1308 is located 2800 km from the mouth of Hudson Strait and represents a distal location for deposition by icebergs originating from the Labrador Sea. Heinrich layers are relatively thin in distal deposits, and consequently, bioturbation can easily blur the signal or obliterate internal structure of the event. To assess stratigraphic integrity and resolution, we used X-ray computed tomography (X-ray CT) to conduct a detailed analysis of sediment structure and bioturbation by examining 1 mm slices of cores from multiple holes at Site U1308. Core scanning XRF was conducted at 1 mm in Holes U1308A, U1308B, and U1308C, and discrete samples at 5 mm intervals were taken from Hole U1308A for IRD and foraminiferal point counting, faunal assemblages, mineralogy (X-ray diffraction, XRD), and stable isotope analysis.

2. Heinrich Terminology

The literature is confounded by different usages of the terms Heinrich layer (HL), Heinrich event (HE), and Heinrich stadial (HS). Following suggestions from other authors [*Barker et al*., 2009; *Sanchez Goñi and*

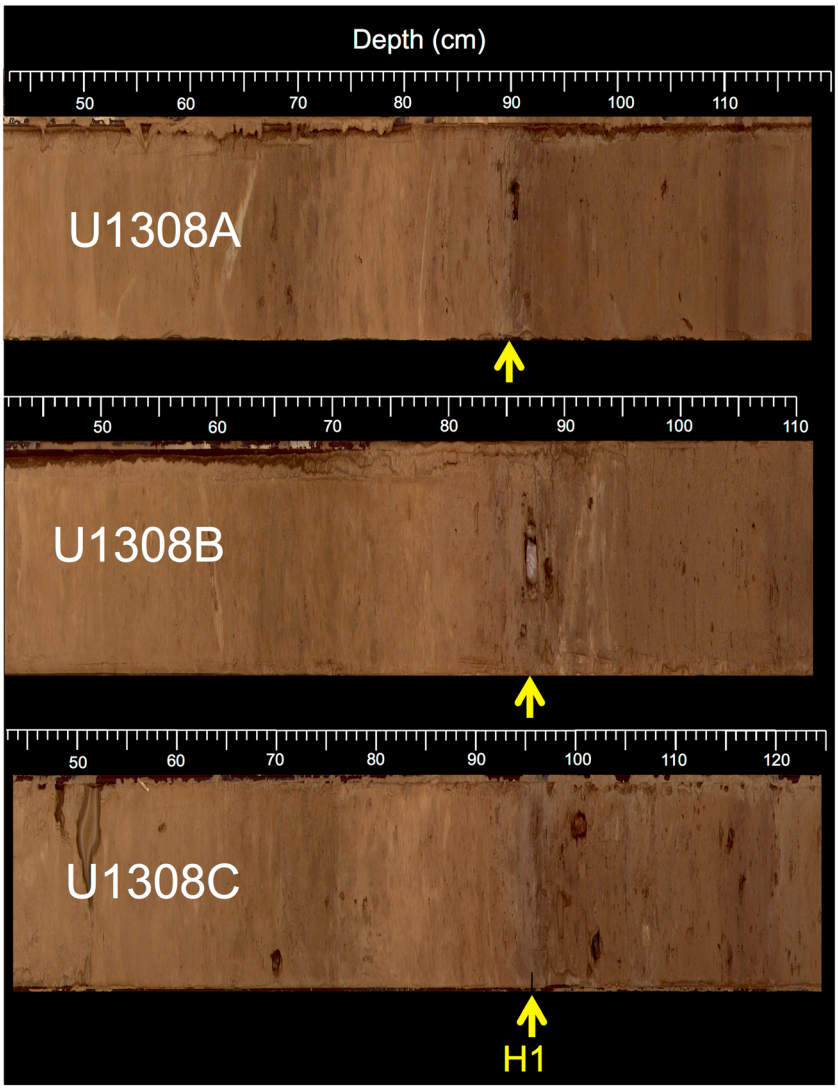

Figure 2. Images of Core 1, Section 1 from Holes U1308A, U1308B, and U1308C. Yellow arrows indicate the base of Heinrich Layer 1 (H1). The dark layer below H1 is rich in manganese.

Harrison, 2010], we adopt consistent definitions and usage of these terms throughout this paper as described below. A Heinrich event (sensu stricto) is the climate event produced by a massive discharge of the Laurentide Ice Sheet through Hudson Strait. Heinrich events occurred during some but not all stadials, which were part of millennial-scale Dansgaard-Oeschger (D-O) oscillations during the last glaciation. A Heinrich layer is the physical manifestation of a Heinrich event preserved in a marine sediment core. A Heinrich stadial is the cold period that contains the Heinrich event. For the last deglaciation, Heinrich Stadial 1 is synonymous with the "Mystery Interval" (17.5 to 14.5 ka) [*Broecker and Barker*, 2007]. A Heinrich event and Heinrich stadial are not the same because Heinrich events are shorter in duration than the Heinrich stadials in which they occur.

3. Results

3.1. Core Images

Heinrich Layer 1 was recovered in IODP Holes U1308A, U1308B, and U1308C and in two holes at DSDP Site 609. All core images show similar features including a sharp color contrast at the base (Figure 2 and supporting information), representing the contact between light colored carbonate-rich sediment of the

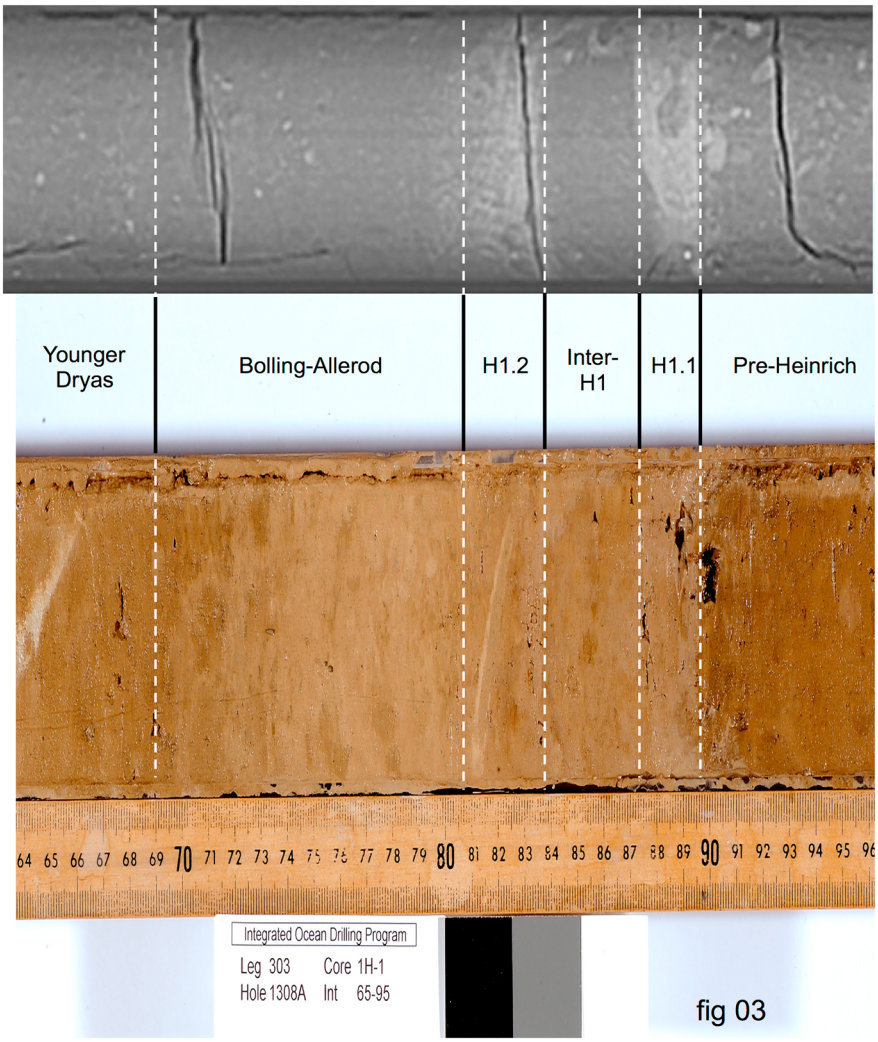

Figure 3. X-ray CT and split core images of Section U1308A-1H-1 showing the various climatic subdivisions of the core.

Heinrich layer and a dark layer below that is rich in manganese. Heinrich Layer 1 is overlain by lighter colored sediments deposited during the Bølling-Allerød (B-A) followed by a transition to the Younger Dryas (Y-D).

3.2. X-Ray CT Images

X-ray CT images were acquired for Holes U1308A and U1308B (see supporting information) but could not be obtained for U1308C because of heavy sampling of both archive and working halves of the core. The CT images reflect density contrasts such that ice-rafted detritus has a greater density than the background pelagic sediments that consists mostly of nannofossil ooze and clay [*Expedition 303 Scientists*, 2006]. Two dense layers are distinctly visible in the CT scan of Hole U1308A, whereas a single mixed layer occurs in Hole U1308B (Figure 3 and supporting information). We refer to the lower peak as H1.1 and the upper peak as H1.2 to distinguish them from H1a and H1b defined by *Bard et al*. [2000] because we are not certain they represent the same events. Each Heinrich layer is poorly sorted, consisting of coarse-grained clasts of IRD embedded in a dense fine-grained matrix. Some large millimeter-sized clasts of IRD are visible in the dark layers immediately below the base of the Heinrich layer in both holes.

Density was calculated for each 1 mm X-ray CT slice in Hole U1308 by averaging the gray scale of all pixels after removing holes and cracks from each slice (Figure 4; see supporting information). In Hole U1308B, the lower layer is up to 2 cm thick, whereas the upper layer is 1 cm thick and the top is bioturbated. The layers also correspond to increases in wet bulk density of the core measured during Expedition 303 by gamma ray attenuation (GRA), which reaches 1.8 g cm^{-3} in each of the two peaks of H1 in Hole U1308A (Figure 4)

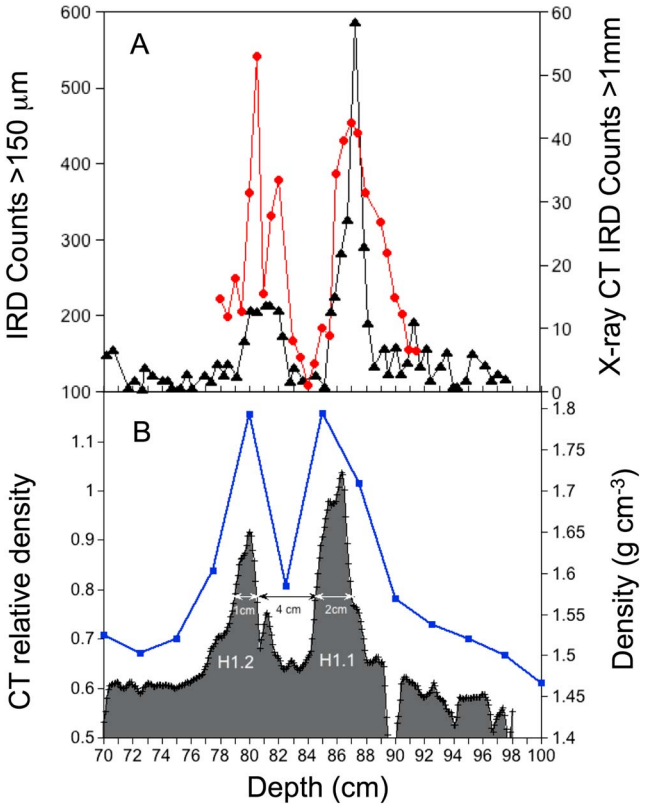

Figure 4. (a) Comparison of IRD point counts from the >150 μm fraction (black) and IRD > 1 mm estimated by image analysis of the X-ray CT images (red). (b) Density estimated by CT core scanner (filled gray area) and gamma ray attenuation (blue) for Section U1308A-1H-1 between 70 and 100 cm. The sediment thicknesses at half peak of H1.1 and 1.2 and the intervening interval are indicated.

[*Expedition 303 Scientists*, 2006]. The GRA was measured at 2.5 cm intervals in Hole U1308A, and the peaks are defined by single points, and fine-scale structure is not captured.

The number of grains of IRD in the CT images was automatically counted using FIJI (ImageJ) software [*Schindelin et al*., 2012] by thresholding each 1 mm slice to exclude fine-grained, low-density matrix sediment and isolate individual IRD grains (Figure 4). IRD grains (>1 mm in size) that were large enough to cross images consisting of 1 mm slices were counted. Grains were counted using a plug-in for FIJI called BoneJ [*Doube et al*., 2010], which hosts an object counter called Particle Analyzer. The plug-in is extremely efficient at quantifying the particles in an image stack but only recognizes particles that span more than one image (i.e., >1 mm in size). IRD counts were binned in 5 mm intervals so that they could be compared with actual counts of IRD obtained from the >150 μm fraction in discrete samples taken every 5 mm (see section 3.4). The pattern of the automated grain counts of >1 mm shows two distinct peaks as do the IRD counts from the >150 μm fraction (Figure 4).

3.3. X-Ray Fluorescence Core Scanning

The quality of XRF data is highly dependent on the physical properties of the sediment core (e.g., varying porosity) [*Grützner and Higgins*, 2010; *Röhl and Abrams*, 2000] and condition of the split core sediment surface and is affected by mineral heterogeneities and surface roughness [*Tjallingii et al*., 2007]. This is particularly problematic for sediment containing IRD because a single grain at the surface can cause large anomalies in elemental variations. Comparison of XRF scans in multiple holes is necessary to evaluate the reproducibility and integrity of the XRF results.

Hodell et al. [2008] demonstrated that Ca/Sr is a reliable proxy for the concentration of detrital carbonate at Site U1308. HL1 is marked by increases in Ca/Sr in all three holes, but subtle differences exist in the structure of the signal among holes (Figure 5). In Hole U1308A, HL1 consists of two sharp peaks in Ca/Sr corresponding with the density peaks in the CT images. The lower, older (H1.1) peak is the stronger of the two and is about 2 cm wide, whereas the upper, younger (H1.2) peak is 1 cm wide. The two peaks are separated by about 3 cm of intervening sediment that contains no detrital carbonate. In Hole U1308B, HL1 consists of a single diffuse Ca/Sr peak that is spread over 7 cm. In Hole U1308C, HL1 consists of two peaks including a larger older peak and smaller second peak separated by less than a centimeter of sediment. The second peak is much weaker and less well defined in Hole U1308C than it is in U1308A. There is also some indication that HL 2 may be double peaked (Figure 5), but we have not studied this event in any detail.

Si/Sr reflects the relative contribution of silicate-rich IRD (Si) and biogenic carbonate (Sr) and has been shown to correlate well with %lithics or total lithics per gram at Sites 609 and U1308 [*Hodell et al*., 2008; *Obrochta et al*., 2014]. High Si/Sr values indicate increased abundance of silicate-rich IRD at Site U1308 [*Hodell et al*., 2008]. Si/Sr is high within both DC-rich layers of Heinrich 1 and is also elevated in the interval leading up

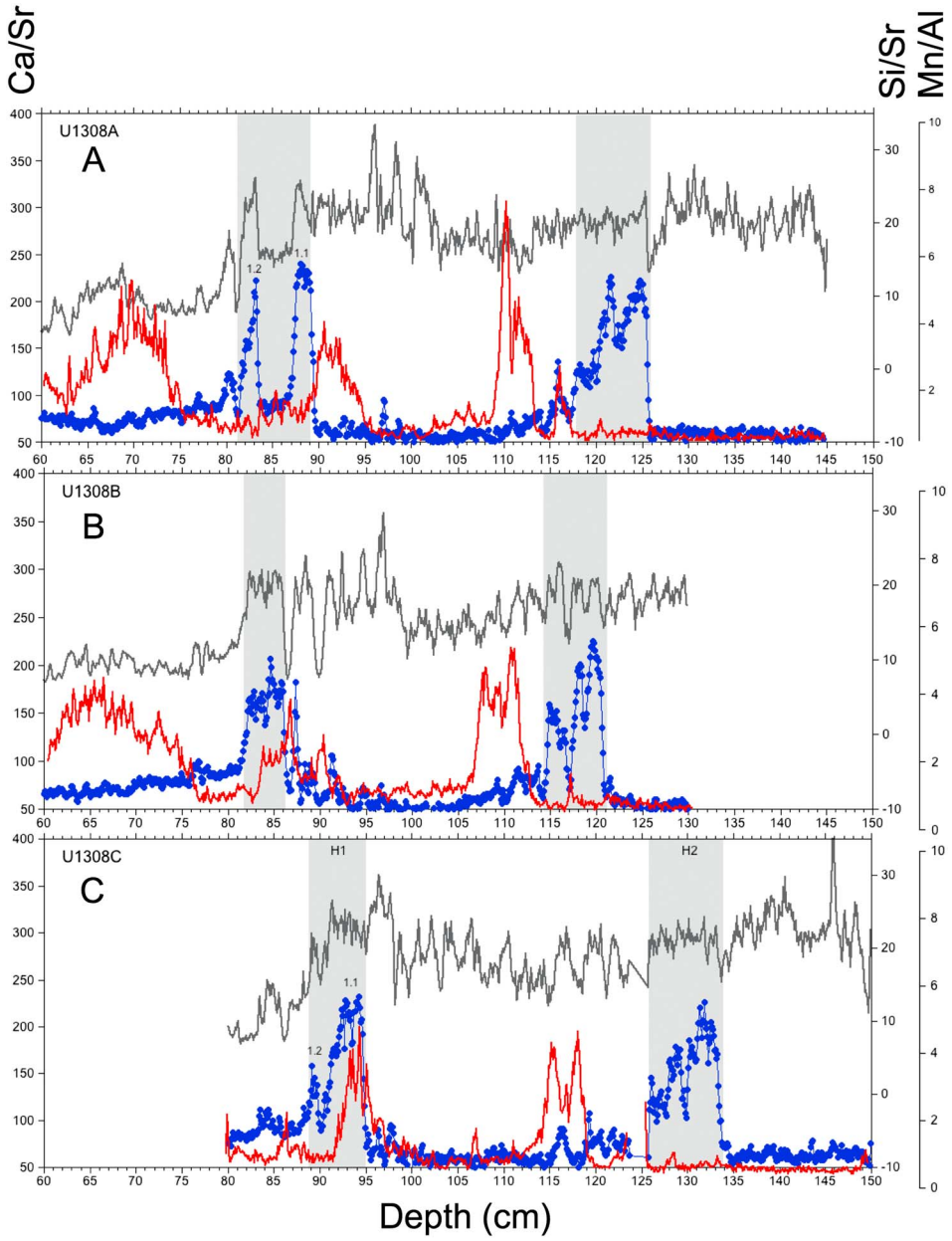

Figure 5. Ca/Sr (blue), Si/Sr (gray), and Mn/Al (red) measured at 1 mm resolution by core scanning XRF for Holes (a) U1308A, (b) U1308B, and (c) U1308C. Gray shading designates the positions of Heinrich Events 1 (H1) and 2 (H2). Note the differences in the shapes and number of the Ca/Sr peaks that is attributed to bioturbation.

to H1 (Figure 5). There is an increase in Si/Sr at 97 cm in Hole U1308B and 107 cm in Hole U1308A during HS1, which define the end of the Last Glacial Maximum and beginning of Heinrich Stadial 1.

Mn/Al shows three peaks in the top 150 cm of Site U1308. Two peaks occur between Heinrich Layers 1.1 and 2 with one peak above H2 and the other near the base of HL1.1 (Figure 5). The third peak occurs at about 65–70 cm above HL1.2.

3.4. XRD and Point Counting

Point counting of the >150 μm size fraction in Hole U1308A confirmed the two peaks in DC (Figures 6 and 7), corresponding to the IRD layers that are observed in the CT images and recorded by elemental ratios (Ca/Sr) measured using the XRF scanner (Figure 5). In Hole U1308A, % total IRD counts begin to increase between 88 and 88.5 cm. A peak in quartz at 89–89.5 cm precedes the increase in detrital carbonate at 87–88 cm (Figure 6)

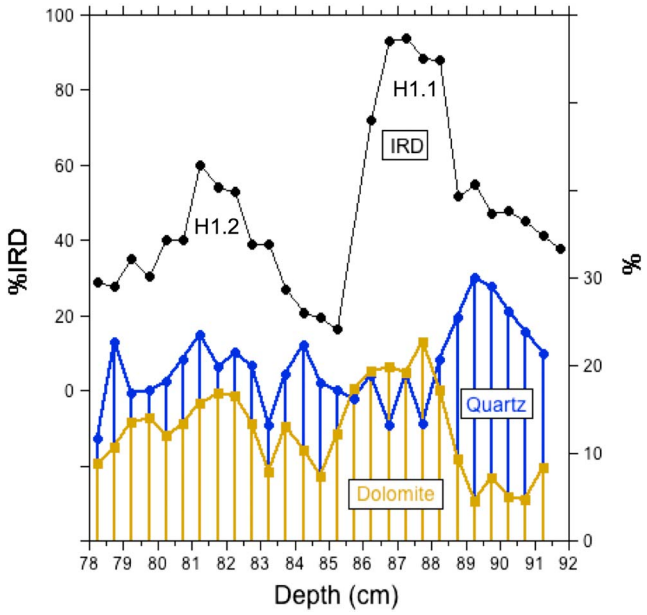

Figure 6. %IRD in the >150 μm size fraction determined by point counting in Section U1308A-1H-1. %Dolomite and Quartz were determined by XRD of bulk sediment (*Allmann and Hinek*, 2007; *Madsen and Scarlett*, 2008; *Cohelo*, 2007). The peak in %quartz at 89–90 cm is a precursor to Heinrich Events 1.1 and 1.2 that are marked by the peaks in %IRD and dolomite.

and corresponds with a peak in Si/Sr (Figure 5). This early IRD is rich in quartz and may represent a "precursor event" as observed at other sites in the North Atlantic [*Grousset et al.*, 2001].

A double peak also occurs in detrital carbonate and IRD during H1 at Site 609 [*Bond et al.*, 1992, 1993; *Bond and Lotti*, 1995], but the sampling resolution at Site 609 was 1 cm rather than 0.5 cm used at Site U1308. Nonetheless, two peaks in % detrital carbonate at 78.5 and 81.5 cm at Site 609 match the peaks at Site U1308 (see supporting information). The lower IRD layer is the thicker of the two and has a greater concentration of IRD grains and dolomite.

3.5. Planktonic Foraminiferal Assemblages

Planktonic foraminifera were counted using standard methods [*Vautravers et al.*, 2004; *Vautravers and Shackleton*, 2006] following the taxonomy of *Kennett and Srinivasan* [1983]. Foraminiferal assemblages are nearly 100% *N. pachyderma* (sin) below HL1 (Figure 8). The abundance of foraminifera is at a minimum, and % *N. pachyderma* (sin) remains near 100% during HL1.1. Toward the top of HL1.1 at 86.5 cm, the percentage of *N. pachyderma* (sin) declines abruptly as the temperate planktonic foraminifera increase, indicating a rapid warming of surface waters. The sediment between the two IRD peaks of H1 contains abundant foraminifera consisting of a temperate water assemblage with relatively low percentages of *N. pachyderma* (sin), averaging 30% of the total assemblage. A small increase in *N. pachyderma* (sin) and decrease in foraminiferal abundance is associated with the younger IRD peak (H1.1) at 82.0 cm.

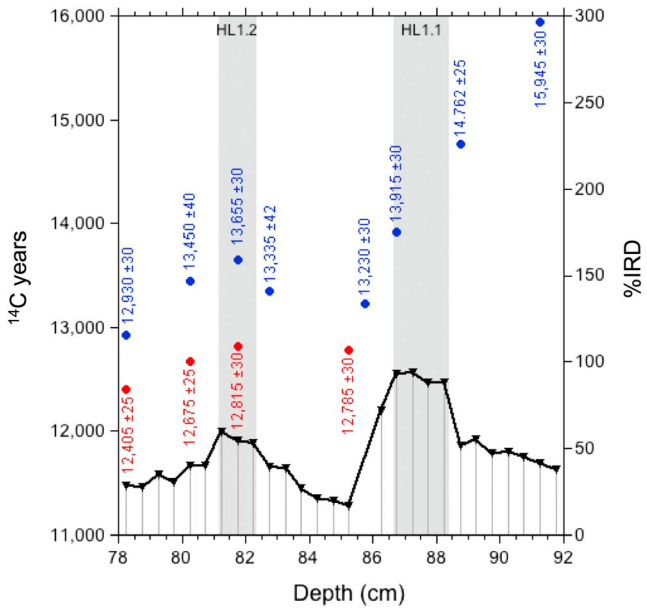

Figure 7. Radiocarbon dates for *N. pachyderma* (sin) (blue) and *G. bulloides* (red) in Section U1308A-1H-1 relative to percent ice-rafted detritus. The peaks of HL1.1 and HL1.2 are indicated by gray shading.

3.6. Stable Isotopes

The $\delta^{18}O$ of bulk carbonate was measured using the method of *Spötl and Vennemann* [2003] and reflects the relative proportion of detrital and biogenic carbonate [*Hodell and Curtis*, 2008] and shows two distinct lows during HL1, reaching minimum values at 87.5 and 82.5 cm (Figure 9). Bulk carbonate oxygen isotopes have negative values reaching as low as −5‰. These values are outside the range of biogenic carbonate seen at Site U1308 and are diagnostic of detrital carbonate derived from Hudson Strait [*Hodell and Curtis*, 2008].

The $\delta^{18}O$ of *N. pachyderma* (sin) decreases below the base of HL1 beginning ~90 cm and reaches minimum values at 87.25 cm in Hole U1308A

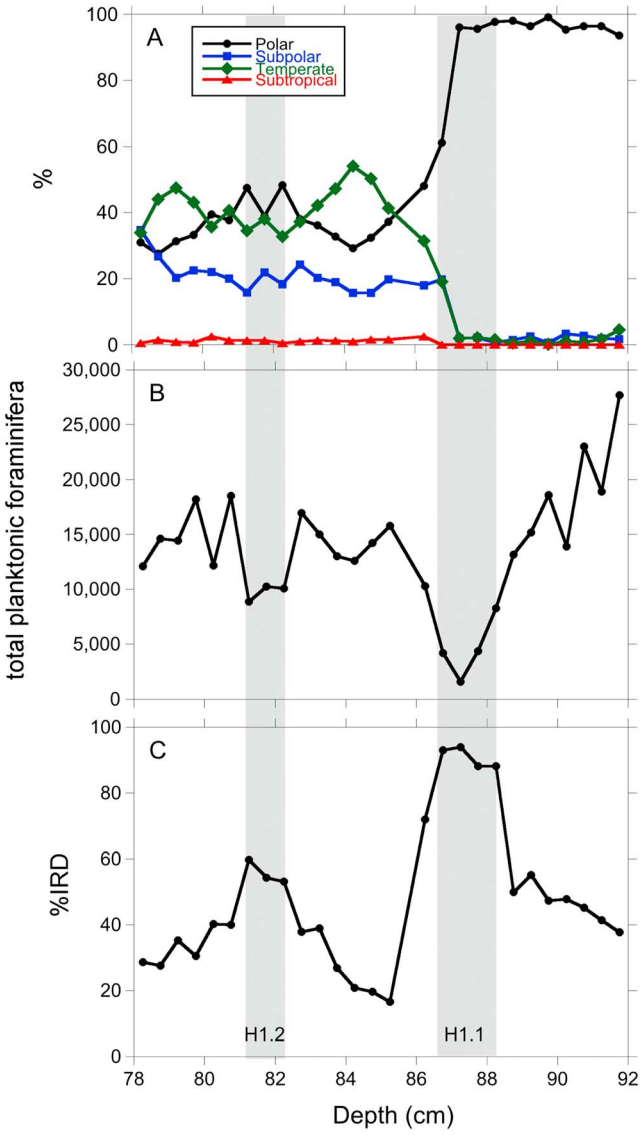

Figure 8. Foraminiferal abundances and %IRD in Section U1308A-1H-1. (a) % faunal assemblages species of total foraminifera: polar = *N. pachyderma* (s); subpolar = *T. quinqueloba* + *G. glutinata* + *G. bulloides*; temperate/transitional = *G. inflata* + *N. pachyderma* (d) + *G. scitula*; and subtropical = *G. falconensis* + *G. rubescens* + *G. ruber* + *G. truncatulinoides* + *H. aequilateralis* + *B. digitata*. (b) Total number of whole foraminifer shells of size >150. (c) % IRD in total (= IRD + others) particles >150 μm.

(Figures 9 and 10). Oxygen isotope values increase slightly in the interval between HL1.1 and HL1.2. The $\delta^{18}O$ of Hole U1308A is very similar to the records from Holes U1308C and 609 (Figure 10).

Benthic $\delta^{18}O$ also decreases across the base of HL1 marking the start of deglaciation (Figure 10). At Hole U1308A, the detrital carbonate peaks are marked by two minima in benthic $\delta^{18}O$. Benthic $\delta^{13}C$ decreases prior to HL1.1 and remains low through HL1.1 and HL1.2 before increasing at the start of the Bølling-Allerød.

3.7. Bioturbation

Bioturbation was studied by digital image analysis [*Dorador and Rodríguez-Tovar*, 2014; *Dorador et al.*, 2014a, 2014b; *Rodríguez-Tovar and Dorador*, 2015] in Holes U1308A and U1308B to determine why Hole U1308A records a distinct double peak, whereas U1308B has a broad single peak. Hole U1308B has a greater overall abundance of large traces fossils and greater bioturbation index than Hole U1308A (Figure 11). *Thalassinoides* is more abundant in Hole U1308B than it is in U1308A, whereas *Planolites* is more dominant at Hole U1308A than U1308B. Hole U1308A contains some intervals with a bioturbation index of 0 (bioturbation absent) that is not observed at Site U1308B. Importantly, the interval between HL1.1 and HL1.2 (intervals 12 and 13 in Figure 11) in Hole U1308A is lacking trace fossils, whereas the corresponding interval in Hole U1308B contains large traces of *Thalassinoides* (Figure 11).

Our bioturbation analysis suggests that the distinct double peak in Hole U1308A was primary in origin and not caused by upward dispersal of detrital carbonate from the lower peak by bioturbation. Moreover, the absence of a double peak in Hole U1308B is attributed to bioturbational disturbance that has mixed the two peaks. We therefore focused our efforts on Hole U1308A because it has been less affected by bioturbation than Hole U1308B.

3.8. Radiocarbon Ages

Radiocarbon dating was performed in Section U1308A-1H-1 across HL1.1 and HL1.2 to constrain the ages of the two IRD layers. The polar form *N. pachyderma* was measured in eight samples, and *G. bulloides* was analyzed in four samples. The ages of *N. pachyderma* are consistently older than *G. bulloides* at the same stratigraphic level by an average of 650 years (Figure 7 and Table 1). Radiocarbon ages decrease from 92 to 86 cm and remain relatively constant from 86 to 80 cm before decreasing again to 78 cm (Figure 7).

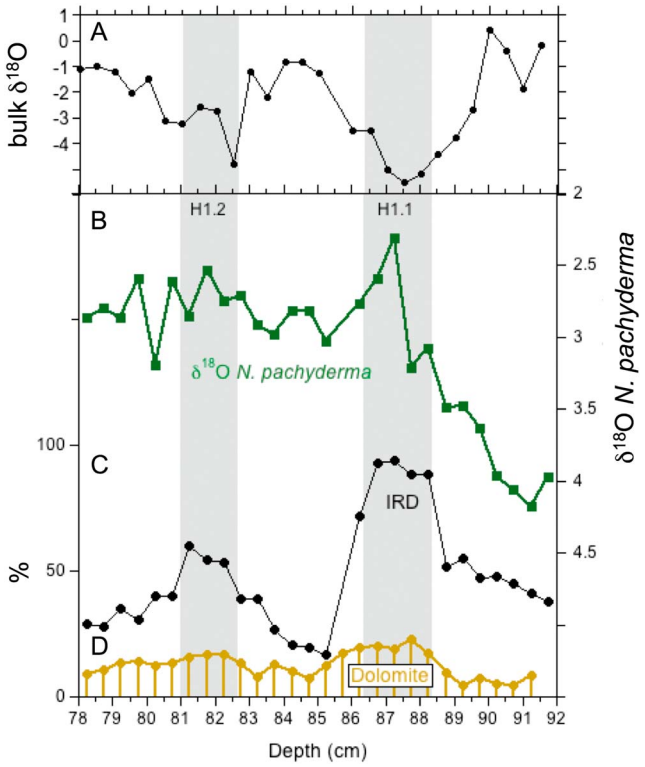

Figure 9. (a) The $\delta^{18}O$ of bulk carbonate (black) and (b) *N. pachyderma* (green) compared to (c) % IRD and (d) % dolomite in Section U1308A-1H-1.

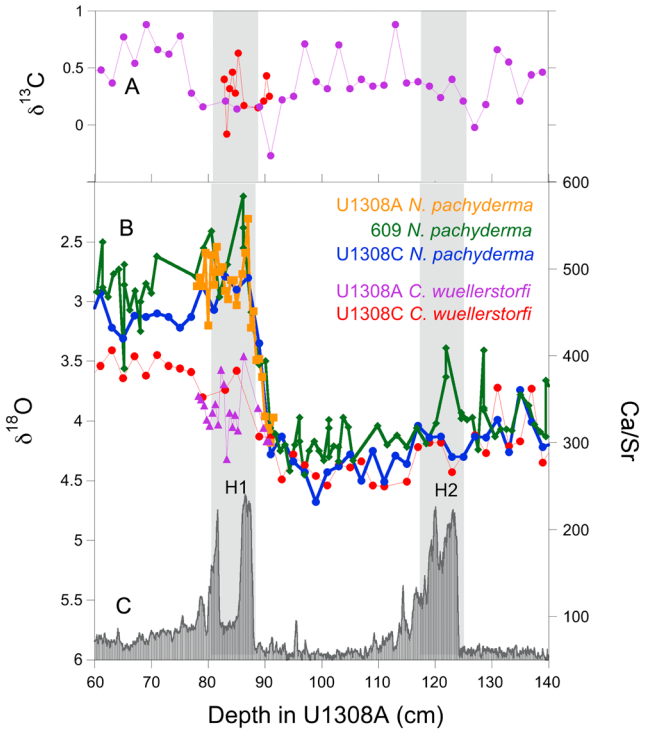

Figure 10. Comparison of (a) benthic carbon and (b) oxygen isotope records of foraminifera at Site U1308 with (c) Ca/Sr indicating detrital carbonate-rich IRD events.

The lower DC layer (H1.1) has a sharp base indicating little mixing of material from below the IRD layer (Figures 2 and 3). The uncorrected radiocarbon age obtained just below the increase in IRD is 14,762 ± 45 $\Delta^{14}C$ years B.P. at 88.5–89 cm (Figure 7). The calendar age is dependent upon the assumption made for the reservoir age correction [*Reimer et al.*, 2013]. It is likely that reservoir ages in the glacial North Atlantic were significantly greater than the modern value of 400 years during Heinrich Stadial 1. *Stern and Lisiecki* [2013] suggested that the reservoir age in the North Atlantic during the early deglacial increased to >1000 ^{14}C years between 18.5 and 16.5 kyr B.P. *Sarnthein et al.* [2015] suggested a reservoir age of 1300 to 1650 ^{14}C years during HS-1 in the subtropical North Atlantic. Assuming a reservoir age of 1200 years [*Stern and Lisiecki*, 2013], the calibrated age at 88.5–89 cm is between 16.2 and 16.5 ka (2 sigma), suggesting that the onset of H1.1 is younger than this age range. This represents a maximum age because bioturbation is suppressed by rapid deposition of the Heinrich layer [*Manighetti et al.*, 1995]. The next dated level at 86.5 to 87 cm occurs where the %IRD is high but *N. pachyderma* (s) has decreased to 60%. The radiocarbon age of 13,915 ± 30 ^{14}C years gives an age range of 15.6 to 15.2 (2 sigma) assuming a 1000 year reservoir age. This represents a minimum age because Heinrich layers are virtually devoid of foraminifera and downward bioturbation of foraminifera from above is likely (Figure 8b) [*Manighetti et al.*, 1995].

The younger DC layer (H1.2) occurs at 81.5 cm with a radiocarbon date of 13,355 ± 42 $\Delta^{14}C$ years B.P. at 82.5–83 cm just below its base (Figure 7). The calibrated age is between 15.6 and 15.2 ka assuming a reservoir age of 500 years for this time period [*Stern and Lisiecki*, 2013] (Table 1). HL1.2 has a sharp base but shows evidence of bioturbation at the top of the layer (Figure 11). Radiocarbon ages at 81.75 cm from the peak of HL1.2 are

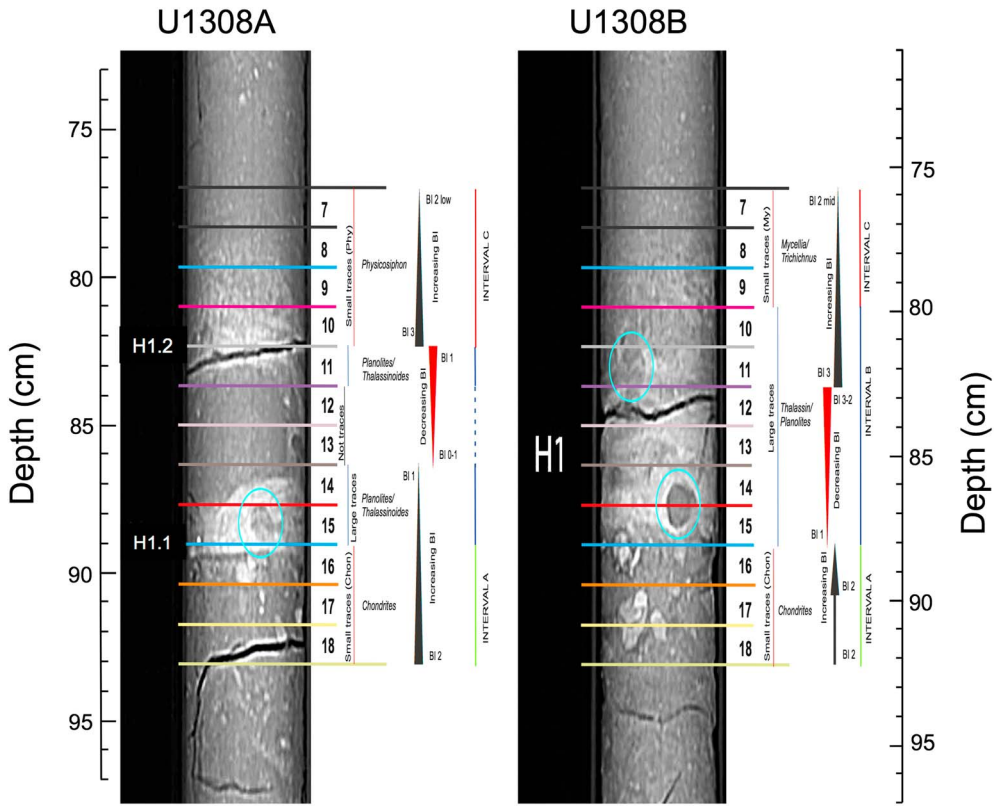

Figure 11. Trace fossil distribution and bioturbation index (BI) in the studied Holes U1308A and U1308B, through the differentiated intervals 18 to 7. Note the absence of discrete trace fossils in intervals 12 and 13 (BI = 0) of Hole U1308A and the presence of *Thalassinoides* and *Planolites* (BI = 2–3) in the corresponding intervals in Hole U1308B.

13,655 ± 30 ^{14}C years B.P. for *N. pachyderma* and 12,815 ± 30 ^{14}C years B.P. for *G. bulloides*. The calibrated age range for *N. pachyderma* is 16 to 15.6 ka assuming a 500 year reservoir age and 15.2 to 14.8 ka assuming a 1000 year reservoir age. Radiocarbon dates for *G. bulloides* suggest a younger age (13.9 to 13.7 ka) for HL1.2 that is within the Bolling-Allerod. *N. pachyderma* (sin) and *G. bulloides* may have different reservoir ages given that the environmental tolerances and depth habitats differ between the two species. Alternatively, specimens of *G. bulloides* may have been mixed down into HL1.2 from the Bolling-Allerod interval above [*Manighetti et al.*, 1995]. The similar ages of both foraminiferal species between 86 and 81 cm may reflect rapid deposition between HL1.1 and 1.2 or a radiocarbon plateau identified by *Sarnthein et al.* [2015] between 16.05 and 15.25 ka (Figure 7). The plateau presents difficulty in accurately dating HL1.2.

Table 1. Radiocarbon Dates in Section U1308A-1H-1[a]

Laboratory ID	Hole-Core-Section	Depth (cm)	Species	^{14}C Years (Uncorrected)	±
180648	U1308A-1H-1	78.25	*N. pachyderma (s)*	12,930	30
180649	U1308A-1H-1	78.25	*G. bulloides*	12,405	25
180650	U1308A-1H-1	80.25	*N. pachyderma (s)*	13,450	40
180651	U1308A-1H-1	80.25	*G. bulloides*	12,675	25
180652	U1308A-1H-1	81.75	*N. pachyderma (s)*	13,655	30
180653	U1308A-1H-1	81.75	*G. bulloides*	12,815	30
1517.1010	U1308A-1H-1	82.75	*N. pachyderma (s)*	13,355	42
180655	U1308A-1H-1	85.25	*G. bulloides*	12,785	30
180654	U1308A-1H-1	85.75	*N. pachyderma (s)*	13,230	30
180656	U1308A-1H-1	86.75	*N. pachyderma (s)*	13,915	30
1517.1010	U1308A-1H-1	88.75	*N. pachyderma (s)*	14,762	45
180657	U1308A-1H-1	91.25	*N. pachyderma (s)*	15,945	35

[a]Foraminiferal specimens were cleaned using a modified version of the clay and organic removal cleaning steps of *Barker et al.* [2003].

The radiocarbon dates from Hole U1308A (Table 1) agree well with radiocarbon ages reported by *Bond et al.* [1992] for Site 609 (see supporting information). At Site 609, the two detrital carbonate peaks occur at 81.5 and 78.5 cm and the nearest radiocarbon dates are at 84–85 cm (14,990 ± 230) and 79–81 cm (13,650 ± 90). The radiocarbon dates from Site 609 are in close agreement with the basal dates for H1.1 (14,762 ± 45) and H1.2 (13,355 ± 42) obtained for Hole U1308A.

We produced a radiocarbon age model by combining dates on *N. pachyderma* from Site U1308 with similar analyses from Site 609 [*Bond et al.*, 1992]. The two sites were correlated precisely to one another using color reflectance [*Hodell et al.*, 2008; *Obrochta et al.*, 2012, 2014]. We used estimates of high-latitude North Atlantic reservoir ages and errors given by *Stern and Lisiecki* [2013]. The age model was developed with Bacon [*Blaauw and Christen*, 2011], which uses Bayesian statistics to reconstruct the accumulation history of the profile. Errors in both radiocarbon calibration and estimation of reservoir age are considered. Results include the mean, median, maximum, and minimum ages for each level in the profile (see supporting information). The age model likely overestimates the duration of HL1.1 and 1.2, which were deposited rapidly and likely lasted for only a few hundred years [*Francois and Bacon*, 1994; *Thomson et al.*, 1995; *McManus et al.*, 1998].

The peak of HL1.1 is estimated at 16.2 ka with a 2 sigma range from 15.5 to 17.1 ka. The age of ~16.2 ka for H1.1 agrees well with estimates of 16.13 ± 0.12 ka from an ice core drilled into the West Antarctic Ice Sheet (WAIS) [*Rhodes et al.*, 2015], 16.2 ka from the Cariaco Basin off Venezuela [*Deplazes et al.*, 2013], and 16.07 ka from Hulu Cave, China [*Treble et al.*, 2007; *Southon et al.*, 2012; *Zhang et al.*, 2014]. The peak of HL1.2 is estimated at 15.1 ka with a range of 14.3 to 15.9 ka. The age model gives an age of 14.7 ka for the base of the Bolling-Allerod warming in the core that matches the date obtained in the Greenland ice core chronology [*Svensson et al.*, 2008].

4. Discussion

4.1. IRD in a Dense Fine-Grained Matrix

In Hole U1308A, Heinrich Event 1 consists of two discrete density peaks (Figure 4). The coarse IRD grains of H1.1 and H1.2 are set within a dense matrix of fine-grained sediment, which is expressed in the CT slices by a cloud of high-density material (Figure 3; also see supporting information). We interpret the fine sediment as glacial flour that is released and dispersed from melting icebergs along with coarser-grained material [*Gilbert*, 1990]. Glacial flour or rock flour is clay- and silt-sized sediment produced by mechanical grinding of bedrock by glaciers. Glacial-aged icebergs derived from the Laurentide Ice Sheet likely had a greater proportion of fine-grained carbonate than modern Atlantic icebergs, which are derived mainly from the Greenland Ice Sheet, because of efficient grinding of Paleozoic carbonates that underlie Hudson Strait and Hudson Bay [*Hiscott and Aksu*, 1996; *Hesse and Khodabakhsh*, 2016; *Hesse*, 2016].

Although IRD layers are often identified through properties of the coarse-sediment fraction, the sand fraction is usually a relatively small portion of most glacial-derived sediment, which is typically in the silt and clay size range [*Andrews*, 2000; *Andrews and Principato*, 2002]. This smaller size fraction is missed in counts of coarse-grained IRD but is a major contributor to glacimarine sedimentation. Glacial flour and especially carbonate can remain in suspension for a long time because of its fine grain size and resistance to flocculation. It can be transported to great distances by currents after release from icebergs. As a result, glacial flour was likely widely dispersed throughout the North Atlantic IRD belt during Heinrich events. The glacial flour increases water turbidity during Heinrich events and, together with low temperatures and increased stratification, suppresses primary productivity that would further hinder this fine material from being incorporated into fecal pellets and sinking [*Syvitski*, 1989]. As a result, the wide distribution and low $\delta^{18}O$ values of the detrital carbonate from Hudson Strait are particularly useful for detecting Heinrich events within and outside the margins of the North Atlantic IRD belt [*Hodell and Curtis*, 2008].

Within the poorly sorted IRD layers, the fine-grained glacial flour fills the voids between larger particles resulting in a substantial increase in sediment packing, thereby resulting in high bulk density (Figure 4). The high density may also be a result of partial cementation of Heinrich layers by authigenic dolomite and ankerite [*Tamburini et al.*, 2002]. Heinrich layers were originally described as "cemented marls" in German cruise reports [*Heinrich*, 1988; *Hemming*, 2004], and scanning electron microscope photos of Heinrich

layers at Site U1308 reveal rhombohedral crystals of dolomite, suggesting that at least some of the dolomite is authigenic (see supporting information).

4.2. Twin Peaks

Our results from Hole U1308A indicate that Heinrich Layer 1 consisted of two discrete pulses of IRD (Figure 6). The two peaks are not the result of bioturbation or coring disturbance. The twin peaks are also observed in the low-resolution counts of detrital carbonate of *Bond et al*. [1992] from nearby Site 609, supporting the dual nature of H1 (see supporting information). Other records also exhibit twin peaks for H1 across the North Atlantic indicating that it may be a pervasive feature. For example, Heinrich layers typically feature two peaks in coarse-grained detrital carbonate within the Labrador Sea [*Rashid et al*., 2003]. This pattern has been attributed to the dilution of the middle of a single IRD layer by meltwater input of fine material [*Hesse and Khodabakhsh*, 1998, 2016; *Clarke et al*., 1999; *Rashid et al*., 2003]. However, a record from sediment core GGC31 on the crest of Orphan Knoll (water depth 1796 m) also shows the pattern of two peaks in detrital carbonate as observed at Site U1308 [*Bond and Lotti*, 1995]. This core is relatively shallow, and located on an isolated high, and so is not affected by turbidity currents originating from Hudson Strait and is too far from Hudson Strait to be affected by meltwater plumes derived from the ice sheet terminus [*Hesse*, 1989; *Hesse and Khodabakhsh*, 2016]. Similarly, Core EW9302-2JPC (1251 m, 48°47.70′N, 45°05.09′W) on the Flemish Cap also shows two distinct peaks during H1 [*Marcott et al*., 2011]. Site U1302/U1303 at 3600 m water depth on Orphan Knoll also shows a small secondary peak associated with the main H1 event (see supporting information).

Sediment core SU90-09, on the southern fringe of the IRD belt, displays two peaks in the proportion of IRD that is detrital carbonate within H1 [*Grousset et al*., 2001]. A record from core SU81-18 from the Iberian Margin shows two distinct IRD peaks that coincide with those seen at Site U1308, although only the earlier of the two peaks is rich in detrital carbonate [*Bard et al*., 2000]. *Bard et al*. [2000] provided ages of 16.0 (H1a) and 17.5 ka (H1b) for the two peaks, assuming a reservoir age of 400 years for Core SU81-18 on the Iberian Margin. However, *Skinner et al*. [2014] demonstrated that reservoir ages on the Iberian Margin were not a constant 400 years but varied by up to 1800 years during Heinrich Stadial 1. Applying a reservoir correction of $>$1000 years to Core SU81-18 would make H1b significantly younger than 17.5 ka. We suggest that H1b of *Bard et al*. [2000] is synchronous with H1.1 at Site U1308. It is the stronger of the two peaks and likely occurred at 16.1 ± 0.123 ka [*Rhodes et al*., 2015]. It is uncertain whether H1a of *Bard et al*. [2000] corresponds to H1.2 because it does not contain detrital carbonate on the Iberian Margin. Two peaks in IRD are similarly recorded on the Laurentian Fan [*Gil et al*., 2015] and dated at 17.5 and 16 cal kyr B.P. These dates are also based on an age model that used a standard marine reservoir correction of 400 years [*Keigwin et al*., 2005].

4.3. Implication of Twin Peaks for Ice Sheet Dynamics

The two DC-rich IRD layers during H1 in Hole U1308A suggests that rapid iceberg discharge from the Hudson Strait ice stream may have occurred in two stages or, alternatively, it involved two independent ice streams. *Alley and MacAyeal* [1994] predicted that all Heinrich events should have a double-peak structure related to the process of freeze on and incorporation of debris into glacial ice. According to their "binge-purge" model [*MacAyeal*, 1993], ice calved early during the surge is debris laden from the previous freeze-on portion of the binge-purge cycle. When debris-laden basal ice is completely melted off the ice stream, clean icebergs are produced resulting in continued freshwater forcing but a hiatus occurs in IRD deposition, producing a "mid-purge hiatus." After freeze on commences but before the purge ends, IRD flux resumes and continues to the end of the purge. Thus, three stages were proposed by *Alley and MacAyeal* [1994]: (i) the initial IRD output, (ii) a midpurge hiatus devoid of IRD, and (iii) a late purge IRD output. The IRD hiatus occurs because debris-laden basal ice is completely melted from the base of the ice stream during the middle portion of the purge.

Although the two peaks recorded at Hole U1308A appear to support the prediction of *Alley and MacAyeal* [1994] that IRD flux should reach a maximum twice during each Heinrich event, there are aspects that may not fit the model. According to the model, IRD is absent during the midpurge hiatus but meltwater is still produced from the melting of clean bergs. Planktonic foraminifera assemblages in the intervening sediment between H1.1 and H1.2 do not support the presence of cold meltwater at Site U1308 but instead are dominated by subpolar species, especially *G. bulloides* (Figure 8). The warming between H1.1 and H1.2 at Site

U1308 does not preclude the possibility of continued iceberg delivery and cooling in the western Atlantic closer to Hudson Strait, but not in the central North Atlantic.

Another consideration is the time difference between the two peaks. *Alley and MacAyeal* [1994] estimated the total duration of the Heinrich event to be 750 years with the debris hiatus lasting 250 years. The age difference between the base of H1.1 and H1.2 is 1400 radiocarbon years, but the absolute age difference between the two peaks depends upon assumptions about the reservoir correction for each date. If the two events occurred at ~16.2 and 15.1 ka, then 1100 years is longer than the predicted duration of 250 years for the midpurge hiatus. The problem is that the 95% age ranges for HL1.1 (15.5–17.1 ka) and HL1.2 (14.3 to 15.9 ka) overlap. If H1.2 is toward the older age of 15.9 ka, then the duration of the midpurge hiatus would be consistent with the estimate of *Alley and MacAyeal* [1994].

Alternatively, the two peaks may represent rapid iceberg delivery from different ice streams, both of which would be underlain by bedrock containing detrital carbonate. The older and main event involved the Hudson Strait Ice Stream. The younger event could be linked to sources from any number of other ice streams draining the eastern margin of the Laurentide Ice Sheet (Figure 1); for example, *Rashid et al*. [2012] suggested that discharge from the Hudson Strait Ice Stream in H1 was followed by the Cumberland Sound Ice Stream (Figure 1). A potential problem with this suggestion is that ice sheet basins such as those draining Cumberland Sound are 1 to 2 orders of magnitude smaller that the Hudson Bay-Hudson Strait system, making the delivery of very large numbers of icebergs unlikely. Another possibility is the Laurentian Channell Ice Stream (Figure 1), which has a relatively large drainage-basin area [*Dowdeswell et al*., 1995]. However, although the St. Lawrence valley contains limestone, we would also expect other lithologies (e.g., Permian-Carboniferous red beds).

4.4. Warming During HE1

Several studies have reported warming during or preceding Heinrich events either in the surface or subsurface waters [*Jonkers et al*., 2010; *Marcott et al*., 2011; *Naafs et al*., 2013]. Warming in the subsurface has been observed in several models during Heinrich events and has led to the suggestion that subsurface warming may have been responsible for destabilization of grounded ice shelves followed by surging of ice streams [*Hulbe*, 1997; *Hulbe et al*., 2004; *Álvarez-Solas et al*., 2010; *Marcott et al*., 2011; *Bassis et al*., 2017]. A possible problem for models invoking the collapse of extensive floating ice shelves in the delivery of IRD is that strong basal melting, which is common close to ice shelf grounding lines [e.g., *Enderlin and Howat*, 2013; *Rignot et al*., 2013], means that icebergs derived from the floating ice shelves themselves may be largely devoid of basal debris [e.g., *Alley et al*., 2005]. Debris-rich icebergs with significant thicknesses of basal debris more probably come from icebergs sourced from grounded ice streams. Alternatively, ice sheet models can simulate a Heinrich event in response to subsurface warming without the necessity of a floating ice shelf [*Bassis et al*., 2017].

In Hole U1308A, planktonic foraminifera assemblages suggest that cold conditions occurred prior to and during H1.1. Toward the latter part of H1.1 moderate warming of surface water occurred and continued through the intervening period between H1.1 and H1.2 (Figure 8). We suggest that the warming during late H1.1 was related to the breakdown in stratification that occurred once the flux of icebergs was reduced. A slight cooling occurred during H1.2 followed by a return to warm conditions during the Bølling-Allerød.

The cold conditions during H1.1 are consistent with model results indicating widespread cooling of North Atlantic SSTs in the IRD belt during Heinrich events in response to freshwater forcing and expanded winter sea ice. Farther south at Site U1313 (41°N), *Naafs et al*. [2013] found evidence of rapid warming of 2–4°C associated with Heinrich events. At Site 976 in the Alboran Sea on the southern Iberian Margin (36°12.3′N, 4°18.7′W), HS1 is punctuated by a sudden brief warming (~4°C in less than eight centuries) at ~16 ka (Figure 12) [*Martrat et al*., 2014]. Measurement of bulk carbonate $\delta^{18}O$ at Site 976 demonstrates that the warming preceded the decrease in bulk $\delta^{18}O$, which indicates the arrival of fine-grained detrital carbonate during Heinrich Event 1 (Figure 12). Previous studies have shown that meltwater reached the western Mediterranean during Heinrich events [*Sierro et al*., 2005], which likely contained fine-grained detrital carbonate from Hudson Strait [*Hodell and Curtis*, 2008]. Our results indicate a pattern of cooling and sea ice expansion in the high-latitude North Atlantic during H1.1 when warming occurred in the subtropical eastern North Atlantic [*Martrat et al*., 2014]. These results support oceanic forcing and subsurface warming as a

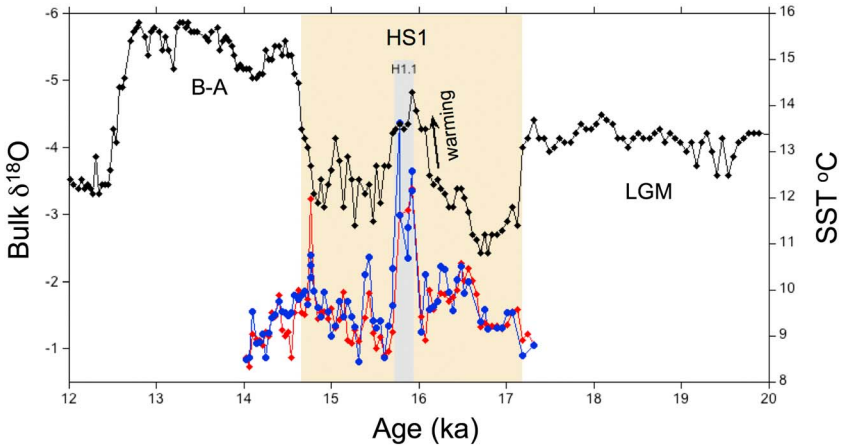

Figure 12. Sea surface temperatures (SSTs) recorded by alkenones [*Martrat et al*., 2014] relative to the $\delta^{18}O$ of bulk carbonate at Site 976 in the Alboran Sea (this study), which we interpret as the delivery of fine-grained detrital carbonate to the site during Heinrich Event 1. The yellow shading defines Heinrich Stadial 1 and gray shading HL 1.1. The bulk carbonate $\delta^{18}O$ was analyzed twice as indicated by the filled circles (blue) and diamonds (red). Note the warming in SST preceded the decrease in bulk carbonate $\delta^{18}O$ and peaks during H1.1.

trigger of Heinrich Event 1 [*Marcott et al*., 2011; *Naafs et al*., 2013] with [*Hulbe*, 1997; *Hulbe et al*., 2004; *Álvarez-Solas et al*., 2010, 2011] or without [*Bassis et al*., 2017] the existence of an ice shelf in the Labrador Sea.

4.5. Relationship of Heinrich Event 1 and Heinrich Stadial 1?

It has been proposed that HE1 occurred when the polar North Atlantic was already cold and AMOC weakened [*Bond et al*., 1992; *McManus et al*., 1994]. Thus, HE1 was not the trigger for Heinrich Stadial 1 but increased freshwater forcing associated with HE1 may have weakened AMOC further. Figure 13 compares Ca/Sr from Site U1308 with Pa/Th from the Bermuda Rise [*McManus et al*., 1994] and Iberian Margin [*Gherardi et al*., 2005]. Overturning circulation in the western Atlantic Basin was suppressed throughout HS1 but was particularly weak during the latter half of HS1. The two detrital carbonate peaks at U1308 correspond with the minima in Pa/Th between ~16 and 15 ka. The Pa/Th record from the Iberian Margin suggests a somewhat different history in that the Pa/Th remains low during the first part of HS1 and increases later than the record from the Bermuda Rise [*Gherardi et al*., 2005, 2009]. On the Iberian Margin, the weakest period of overturning circulation occurs during the period when HL1.1 and HL1.2 were deposited (Figure 13).

Broecker and Putnam [2012] proposed a two-stage subdivision of Heinrich Stadial 1 with a transition at ~16.1 ka. During the early stage of HS1 (18 to 16.1 ka), $\delta^{18}O$ in Greenland ice cores was less negative indicating warmer temperatures than the latter stages of HS1 (Figure 13). The coldest conditions occurred during the latter half of HS1 (16.1 to 14.7 ka). The observation that H1 was not the cause of HS1 raises the question what was responsible for cooling and weakening of overturning circulation in early HS1 prior to the Heinrich event? Several studies show that IRD deposition prior to H1 in the central and eastern North Atlantic was derived mainly from European and Iceland ice sheets [*Grousset et al*., 2001; *Peck et al*., 2006]. *Peck et al*. [2006] suggested that instability and meltwater forcing by the Northwest European Ice Sheet temporarily weakened AMOC prior to HE1, illustrating that even modest ice sheets can have a disproportionate impact on deep-water circulation if the ice sheet is close to the source of deep-water formation. *Toucanne et al*. [2010, 2015] found a significant increase in sediment load to the Bay of Biscay at circa 20 ka that reflects the start of European deglaciation with a pronounced peak in Fleuve Manche discharge at 18 ka (Figure 13). The reduction in AMOC during the early part of HS1 may have been driven by earlier melt from the European ice sheet (~20–16.5 ka) [*Peck et al*., 2006; *Toucanne et al*., 2015], whereas the Laurentide played a more significant role during the latter half of HS1 from 16.5 to 14.7 ka.

4.6. Significance of Manganese Peaks

The base of HL1.1 is sharp and underlain by dark sediment enriched in Mn (Figures 2, 3, and 5). Mn^{2+} is mobile under reducing conditions and precipitates as Mn (III, IV) under oxic conditions. It is typically enriched in oxic sediments with a concentration maximum near the surface where reduced Mn^{2+} migrates from reducing

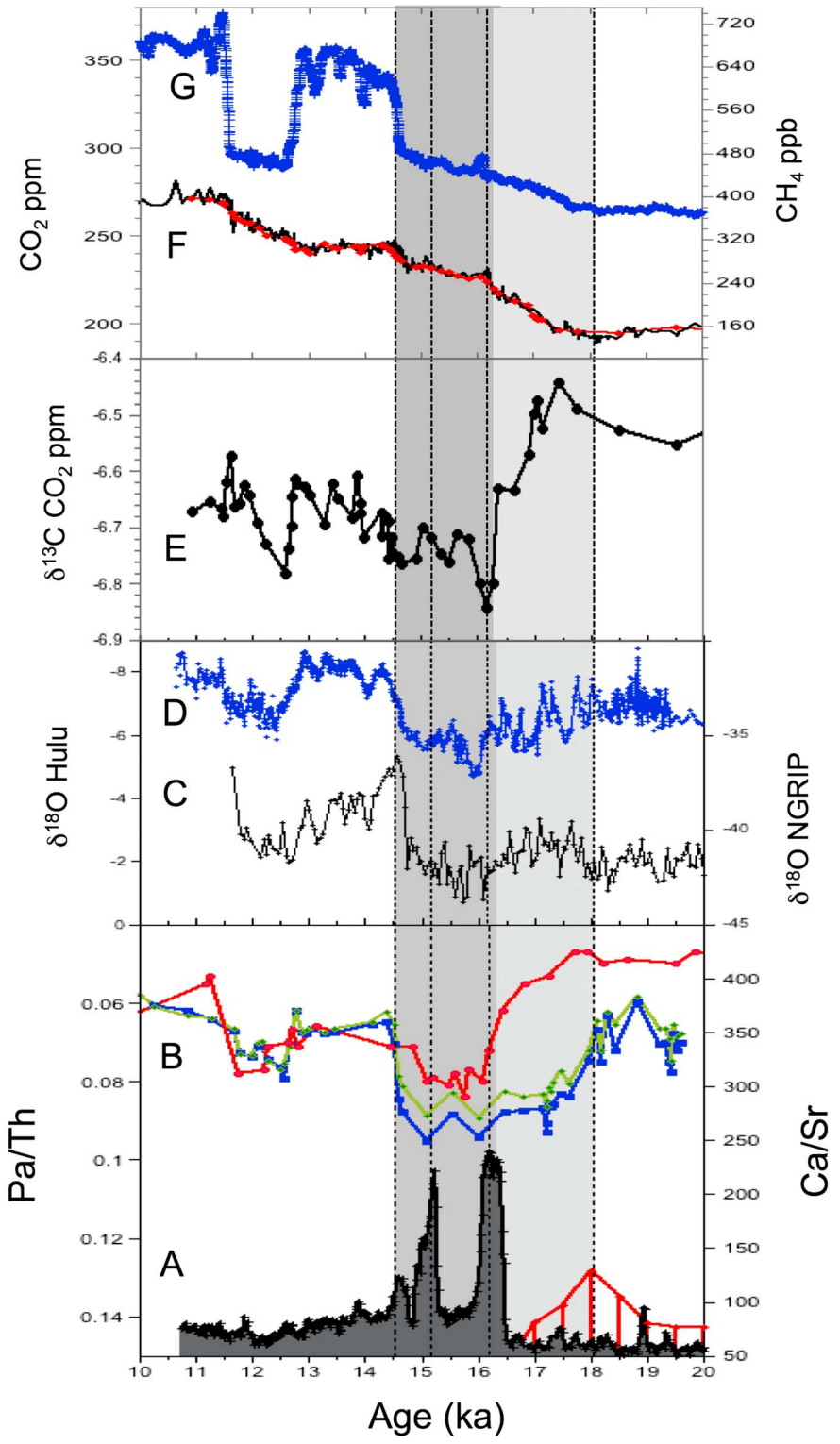

Figure 13. Comparison of (a) Ca/Sr of Site U1308 (filled black) and flux of Fleuve Manche sediment load (red, *Toucanne et al.*, 2010); (b) Pa/Th from the Bermuda Rise (green and blue) [*McManus et al.*, 2004] and Iberian Margin (red) [*Gherardi et al.*, 2005]; (c) the oxygen isotope record of Greenland [*North Greenland Project Members*, 2004]; (d) the oxygen isotope record of Hulu Cave, China [*Wang et al.*, 2001; *Wu et al.*, 2009, on time scale of *Southon et al.*, 2012]; (e) $\delta^{13}C$ of atmospheric CO_2 from Taylor Glacier [*Bauska et al.*, 2016]; (f) CO_2 [*Marcott et al.*, 2014], and (g) CH_4 [*Rhodes et al.*, 2015] from the WAIS Divide ice core. The gray shaded areas denote the two-stage subdivision of HS1 at 16.1 ka as suggested by *Broecker and Putnam* [2012].

sediment below and is oxidized at the redox boundary that occurs near the depth of oxygen penetration into the sediments. Three Mn peaks occur in the upper 150 cm of Site U1308 indicating nonsteady state Mn redox cycling (Figure 5) [*Burdige*, 1993]. We suggest that the two older peaks represent relict Mn-rich layers that formed at former redox boundaries, whereas the uppermost peak is actively forming today. Dissolution of the older Mn peaks may have been retarded by the deposition of HL1, which impeded upward diffusion of Mn^{2+} because of its high density and low porosity.

Manganese peaks are often found at glacial-interglacial transitions suggesting a change in redox conditions [*Mangini et al*., 1990, 1991; *Jaccard et al*., 2016; *Gottschalk et al*., 2016]. Because Mn^{2+} migrates in the sediments, the age of the sediment hosting the Mn peak provides a maximum age of the redox change [*Mangini et al*., 2001]. We suggest that the Mn peak associated with HL1.1 formed by a shoaling of the redox boundary in response to lowered oxygen and diminished ventilation of deep water. Similarly, the oldest Mn peak formed sometime during or after the Last Glacial Maximum. Both peaks are consistent with very old deep-water reservoir ages (between ~2250 and ~3400 years) in the North Atlantic during the Last Glacial Maximum and HS1 [*Skinner et al*., 2014] and with lower oxygen concentrations of deep water on the Iberian Margin especially during HS1 [*Hoogakker et al*., 2015].

In addition to bottom-water oxygenation, several factors can also influence Mn accumulation in marine sediments including changes in organic matter flux and sediment accumulation rate. Certainly, the deposition of the Heinrich layers resulted in large changes in sedimentation rate and we cannot rule out that the enrichment in Mn is a diagenetic consequence of changing sediment or organic fluxes [*Thomson et al*., 1996, 1999] rather than changes in deep-water oxygenation.

4.7. Relationship of Heinrich Event 1 to Deglaciation

It is uncertain whether HE1 was merely a symptom of the last deglaciation or whether it played a more active role in Termination I. For example, HE1 may have led to CO_2 degassing in the Southern Ocean through a bipolar seesaw mechanism [*Sigman et al*., 2007; *Cheng et al*., 2009; *Wolff et al*., 2009; *Denton et al*., 2010; *Skinner et al*., 2014; *Marcott et al*., 2014; *Menviel et al*., 2014], thereby hastening deglaciation. In order to evaluate the importance of the observed changes at Site U1308 across the last deglaciation, we compare our record with ice core records of atmospheric CH_4 [*Rhodes et al*., 2015], CO_2 [*Marcott et al*., 2014], and the $\delta^{13}C$ of atmospheric CO_2 [*Bauska et al*., 2016] (Figure 13).

Rhodes et al. [2015] found a methane spike at 16.1 ka in a WAIS ice core that is not matched by an equivalent increase in Greenland methane. Their interpretation is that CH_4 is sourced from the Southern Hemisphere and occurs during Heinrich events when the ITCZ is driven far south. Thus, the methane event provides a constraint on the age of the Heinrich event and duration of its climate impact. The age of H1 is estimated to be 16.13 ± 0.12 ka, and the duration of the climatic impact is 1515 ± 38 years, which agrees within error of age estimate of HL1.1 at Site U1308/609 (Figure 13).

Marcott et al. [2014] reported a high-resolution record of atmospheric CO_2 for the last deglaciation and defined two modes of change based on rates of CO_2 rise. The first mode is marked by relatively gradual CO_2 rise (10 ppm kyr^{-1}) that occurred from 18.1 to 16.1 ka and 13.0 to 11.5 ka. The second mode of CO_2 change is a series of small, rapid increases during the last termination that occurred at 16.3, 14.8, and 11.7 ka and were synchronous with abrupt increases in CH_4 of the order of ~10 ppm in 100–200 years [*Marcott et al*., 2014] (Figure 13). HL1.1 is associated with the small rapid increases in CO_2 at 16.3 ka. The rapid increases in CO_2 and CH_4 around 16.3 ka correspond to a negative excursion in $\delta^{13}C$ of CO_2 and are associated with H1.1 [*Bauska et al*., 2016]. The $\delta^{13}C$ decrease has been interpreted to represent a rapid release of terrestrial organic carbon as a consequence of drying in the Northern Hemisphere related to Heinrich Event 1 when the ITCZ shifted far to the south (Figure 13) [*Bauska et al*., 2016].

5. Conclusions

We have demonstrated that high-resolution XRF core scanning and CT scanning are valuable tools for evaluating internal structure and bioturbation of Heinrich layers. Hole U1308A is minimally affected by bioturbation in the interval between HL1.1 and HL1.2, indicating the deposition of two distinct layers of IRD that are rich in detrital carbonate. Each detrital layer is composed of poorly sorted, coarse-grained clasts

of IRD embedded in a dense, fine-grained matrix of glacial rock flour that is partially cemented (Figure 3). When sedimentation rates are low and the Heinrich layers are relatively thin, bioturbation can modify or obliterate internal structure of the event, as documented for H1 in Hole U1308B where only a single mixed peak is observed (Figure 11).

A Bayesian age model of radiocarbon dates provides best estimates for the ages of the two peaks: ~16.2 (15.5–17.1) ka for H1.1 and ~15.1 (14.3 to 15.9) ka for HL1.2. Uncertainty in reservoir ages and a plateau in radiocarbon ages between 81 and 86 cm prevent an unambiguous estimate of absolute ages, especially for H1.2 (Figure 7). HL1.1 is clearly the stronger of the two peaks and the estimated age correlates well with climate events recorded in Chinese speleothems [*Treble et al*., 2007], ice cores [*Rhodes et al*., 2015], and the sediments of the Cariaco Basin [*Deplazes et al*., 2013]. HL1.2 is thinner and weaker than HL1.1, and its age is less certain.

The twin peak nature of HL1 is consistent with the model prediction of *Alley and MacAyeal* [1994] that IRD flux should reach a maximum twice during each Heinrich event. However, planktonic foraminifera indicate a moderate warming during the would-be midpurge hiatus period between HL1.1 and 1.2 (Figure 8), which is not predicted by the model. Alternatively, the two peaks could represent discharge of two independent ice streams that are underlain by limestone, although this appears less likely.

Heinrich Stadial 1 marks the start of the last deglaciation and is characterized by cooling in the North Atlantic at the same time as Antarctic temperatures warmed, CO_2 and CH_4 began to increase, $\delta^{13}C$ of CO_2 decreased, and the radiocarbon age of the atmosphere became older [*Broecker and Barker*, 2007; *Marcott et al*., 2014; *Rhodes et al*., 2015; *Bauska et al*., 2016]. Our results suggest a complex history for Heinrich Stadial 1 and support a twofold subdivision suggested by *Broecker and Putnam* [2012] with a transition at 16.1–16.2 ka. Heinrich Event 1.1 occurred midway through Heinrich Stadial 1 when the polar North Atlantic was already cold and overturning circulation weakened. Warming ensued in the subtropical North Atlantic prior to and during H1.1, whereas it was delayed at Site U1308 until the end of H1.1 when the production of icebergs waned and surface water stratification declined. HS1 may have been influenced by melting of European ice sheets during the early phase (~19 to 16.1 ka), whereas Laurentide Ice Sheet dynamics dominated during the latter half of HS1 (16.2 to 14.7 ka).

Acknowledgments
We thank Nick Evans and Giulio Lampronti for XRD analysis and Vera Lukies (MARUM) for assistance with XRF core scanning. David Naafs and an anonymous referee substantially improved the manuscript through their detailed reviews. This research used data acquired at the XRF Core Scanner Lab at the MARUM–Center for Marine Environmental Sciences, University of Bremen, Germany. This research used samples provided by the International Ocean Discovery Program (IODP). Funding for this research was provided by the UK Natural Environmental Research Council (NERC) to Hodell. The *NERC Radiocarbon* Facility supported two radiocarbon dates, and Wally Broecker generously supported the remainder with funding from the Comer Family Foundation. Research by Rodríguez-Tovar and Dorador was financed by Project CGL2015-66835-P. B.M. acknowledges support from the CSIC-Ramón y Cajal postdoctoral programme RYC-2013-14073. J.F.E. would like to acknowledge funding under ERC Advanced grant 320750-Nanopaleomagnetism. All data are archived with Pangaea (https://www.pangaea.de/) and NOAA (https://www.ncdc.noaa.gov/data-access/paleoclimatology-data) information systems.

References

Alley, R. B., and D. R. MacAyeal (1994), Ice-rafted debris associated with binge/purge oscillations of the Laurentide Ice Sheet, *Paleoceanography*, *9*(4), 503–512, doi:10.1029/94PA01008.

Alley, R. B., J. T. Andrews, D. C. Barber, and P. U. Clark (2005), Comment on "Catastrophic ice shelf breakup as the source of Heinrich event icebergs" by C. L. Hulbe et al., *Paleoceanography*, *20*, PA1009, doi:10.1029/2004PA001086.

Allmann, R., and R. Hinek (2007), The introduction of structure types into the Inorganic Crystal Structure Database ICSD, *Acta Cryst*, *A63*, 412–417.

Álvarez-Solas, J., S. Charbit, C. Ritz, D. Paillard, G. Ramstein, and C. Dumas (2010), Links between ocean temperature and iceberg discharge during Heinrich events, *Nat. Geosci.*, *3*, 122–126.

Álvarez-Solas, J., M. Montoya, C. Ritz, G. Ramstein, S. Charbit, C. Dumas, K. Nisancioglu, T. Dokken, and A. Ganopolski (2011), Heinrich event 1: An example of dynamical ice-sheet reaction to oceanic changes, *Clim. Past*, *7*, 1297–1306, doi:10.5194/cp-7-1297-2011.

Andrews, J. T. (2000), Icebergs and iceberg rafted detritus (IRD) in the North Atlantic: Facts and assumptions, *Oceanography*, *13*(3), 100–108.

Andrews, J. T., and K. Tedesco (1992), Detrital carbonate-rich sediments, northwestern Labrador Sea: Implications for ice-sheet dynamics and iceberg rafting (Heinrich) events in the North Atlantic, *Geology*, *20*, 1087–1090.

Andrews, J. T., and S. M. Principato (2002), Grain-size characteristics and provenance of ice-proximal glacial marine sediments (or why do we do grain-size analyses anyway?), in *Glacier Influenced Sedimentation at High Latitude Continental Margins*, vol. 203, edited by J. A. Dowdeswell and C. O'Cofaigh, pp. 305–324, Geol. Soc. London Spec. Publ., Bath, U. K.

Bard, E., F. Rostek, J.-L. Turon, and S. Gendreau (2000), Hydrological impact of Heinrich events in the subtropical Northeast Atlantic, *Science*, *289*, 1321–1324.

Barker, S., M. Greaves, and H. Elderfield (2003), A study of cleaning procedures used for foraminiferal Mg/Ca paleothermometry, *Geochem. Geophys. Geosyst.*, *4*(9), 8407, doi:10.1029/2003GC000559.

Barker, S., P. Diz, M. J. Vautravers, J. Pike, G. Knorr, I. R. Hall, and W. S. Broecker (2009), Interhemispheric Atlantic seesaw response during the last deglaciation, *Nature*, *457*, 1097–1103.

Bassis, J. N., S. V. Petersen, and L. Mac Cathles (2017), Heinrich events triggered by ocean forcing and modulated by isostatic adjustment, *Nature*, *542*, 332–334.

Bauska, T. K., D. Baggenstos, E. J. Brook, A. C. Mix, S. A. Marcott, V. V. Petrenko, H. Schaefer, J. P. Severinghaus, and J. E. Lee (2016), Carbon isotopes characterize rapid changes in atmospheric carbon dioxide during the last deglaciation, *Proc. Nat. Acad. Sci. U.S.A.*, *113*(13), 3465–3470.

Blaauw, M., and J. A. Christen (2011), Flexible paleoclimate age-depth models using an autoregressive gamma process, *Bayesian Anal.*, *6*, 457–474.

Bond, G. C., and R. Lotti (1995), Iceberg discharges into the North Atlantic on millennial time scales during the last glaciation, *Science*, *267*, 1005–1010, doi:10.1126/science.267.5200.1005.

Bond, G. C., W. Showers, M. Elliot, M. Evans, R. Lotti, I. Hajdas, G. Bonani, and S. Johnson (1999), The North Atlantic's 1–2 kyr climate rhythm: Relation to Heinrich events, Dansgaard/Oeschger cycles and the Little Ice Age, in *Mechanisms of Global Climate Change at Millennial Time Scales*, *Geophys. Monogr. Ser.*, vol. 112, edited by P. U. Clark, R. S. Webb, and L. D. Keigwin, pp. 35–58, AGU, Washington, D. C.

Bond, G., et al. (1992), Evidence for massive discharges of icebergs into the North Atlantic Ocean during the last glacial period, *Nature*, *360*, 245–249, doi:10.1038/360245a0.

Bond, G., W. Broecker, S. Johnsen, J. McManus, L. Labeyrie, J. Jouzel, and G. Bonani (1993), Correlations between climate records from North Atlantic sediments and Greenland ice, *Nature*, *365*, 143–147.

Broecker, W., and A. E. Putnam (2012), How did the hydrologic cycle respond to the two-phase mystery interval?, *Quat. Sci. Rev.*, *57*, 17–25.

Broecker, W. S., G. Bond, M. Klas, E. Clark, and J. McManus (1992), Origin of the northern Atlantic's Heinrich events, *Clim. Dyn.*, *6*, 265–273, doi:10.1007/BF00193540.

Broecker, W. S., and S. Barker (2007), A 190‰ drop in atmosphere's $\Delta^{14}C$ during the "Mystery Interval" (17.5 to 14.5 kyr), *Earth Planet. Sci. Lett.*, *256*(1), 90–99, doi:10.1016/j.epsl.2007.01.015.

Burdige, D. J. (1993), The biogeochemistry of manganese and iron reduction in marine sediments, *Earth Sci. Rev.*, *35*, 249–284.

Cheng, H., R. L. Edwards, W. S. Broecker, G. H. Denton, X. Kong, Y. Wang, R. Zhang, and X. Wang (2009), Ice age terminations, *Science*, *326*(5950), 248–252.

Clarke, G. K. C., S. J. Marshall, C. Hillaire-Marcel, G. Bilodeau, and C. Veiga-Pires (1999), A glaciological perspective on Heinrich events, in *Mechanisms of Global Climate Change at Millennial Time Scales*, vol. 112, edited by P. U. Clark, R. S. Webb, and L. D. Keigwin, pp. 243–262, AGU, Washington, D. C.

Cohelo, A. (2007), *TOPAS-Academic*, Coelho Software, Brisbane, Australia.

Denton, G. H. and T. J. Hughes (Eds.) (1981), The Last Great Ice Sheets, 484 pp., John Wiley, New York.

Denton, G. H., R. F. Anderson, J. R. Toggweiler, L. Edwards, J. M. Schaefer, and A. E. Putnam (2010), The last glacial termination, *Science*, *328*, 1652–1656.

Deplazes, G., et al. (2013), Links between tropical rainfall and North Atlantic climate during the last glacial period, *Nat. Geosci.*, *6*, 213–217.

Dorador, J., and F. J. Rodríguez-Tovar (2014), A novel application of digital image treatment by quantitative pixel analysis to trace fossil research in marine cores, *Palaios*, *29*, 533–538.

Dorador, J., F. J. Rodríguez-Tovar, and IODP Expedition 339 Scientists (2014a), Digital image treatment applied to ichnological analysis of marine core sediments, *Facies*, *60*, 39–44.

Dorador, J., F. J. Rodríguez-Tovar, and IODP Expedition 339 Scientists (2014b), Quantitative estimation of bioturbation based on digital image analysis, *Mar. Geol.*, *349*, 55–60.

Doube, M., M. M. Kłosowski, I. Arganda-Carreras, F. P. Cordelieres, R. P. Dougherty, J. S. Jackson, B. Schmid, J. R. Hutchinson, and S. J. Shefelbine (2010), BoneJ: Free and extensible bone image analysis in ImageJ, *Bone*, *47*(6), 1076–1079.

Dowdeswell, J. A., M. A. Maslin, J. T. Andrews, and I. N. McCave (1995), Iceberg production, debris rafting, and the extent and thickness of Heinrich layers (H-1, H-2) in North Atlantic sediments, *Geology*, *23*(4), 301–304.

Enderlin, E. M., and I. M. Howat (2013), Submarine melt rate estimates for floating termini of Greenland outlet glaciers (2000–2010), *J. Glaciol.*, *59*, 67–75.

Expedition 303 Scientists (2006), Site U1308, in *Proc. IODP, 303/306*, edited by J. E. T. Channell et al., Integrated Ocean Drilling Program Management International, Inc., College Station, Tex., doi:10.2204/iodp.proc.303306.108.2006.

Francois, R., and M. P. Bacon (1994), Heinrich events in the North Atlantic: Radiochemical evidence, *Deep Sea Res., Part I*, *41*, 315–334.

Gherardi, J.-M., L. Labeyrie, J. F. McManus, R. Francois, L. C. Skinner, and E. Cortijo (2005), Evidence from the northeastern Atlantic basin for variability in the rate of the meridional overturning circulation through the last deglaciation, *Earth Planet. Sci. Lett.*, *240*, 710–723.

Gherardi, J.-M., L. Labeyrie, S. Nave, R. Francois, J. F. McManus, and E. Cortijo (2009), Glacial-interglacial circulation changes inferred from $^{231}Pa/^{230}Th$ sedimentary record in the North Atlantic region, *Paleoceanography*, *24*, PA2204, doi:10.1029/2008PA001696.

Gil, I. M., L. D. Keigwin, and F. Abrantes (2015), The deglaciation over Laurentian Fan: History of diatoms, IRD, ice and fresh water, *Quat. Sci. Rev.*, *129*, 57–67.

Gilbert, R. (1990), Rafting in glacimarine environments, in *Glacimarine Processes and Sedimentation*, vol. 53, edited by J. A. Dowdeswell and J. D. Scourse, pp. 105–120, Geol. Soc. London Spec. Publ., Bath, U. K.

Gottschalk, J., L. C. Skinner, J. Lippold, H. Vogel, N. Frank, S. L. Jaccard, and C. Waelbroeck (2016), Biological and physical controls in the Southern Ocean on past millennial-scale atmospheric CO_2 changes, *Nat. Commun.*, *7*, 11,539, doi:10.1038/ncomms11539.

Grousset, F. E., E. Cortijo, S. Huon, L. Herve, T. Richter, D. Burdloff, J. Duprat, and O. Weber (2001), Zooming in on Heinrich layers, *Paleoceanography*, *16*(3), 420–259, doi:10.1029/2000PA000559.

Grützner, J., and S. M. Higgins (2010), Threshold behavior of millennial scale variability in deep water hydrography inferred from a 1.1 Ma long record of sediment provenance at the southern Gardar Drift, *Paleoceanography*, *25*, PA4204, doi:10.1029/2009PA001873.

Heinrich, H. (1988), Origin and consequences of cyclic ice rafting in the northeast Atlantic Ocean during the past 130,000 years, *Quat. Res.*, *29*, 142–152, doi:10.1016/0033-5894(88)90057-9.

Hemming, S. R. (2004), Heinrich events: Massive late Pleistocene detritus layers of the North Atlantic and their global climate imprint, *Rev. Geophys.*, *42*, RG1005, doi:10.1029/2003RG000128.

Hesse, R. (2016), Ice-proximal Labrador Sea Heinrich layers: A sedimentological approach, *Can. J. Earth Sci.*, *53*, 71–100.

Hesse, R. (1989), Drainage systems associated with mid-ocean channels and submarine yazoos: Alternative to submarine fan depositional systems, *Geology*, *17*, 1148–1151.

Hesse, R., and S. Khodabakhsh (1998), Depositional facies of late Pleistocene Heinrich events in the Labrador Sea, *Geology*, *26*, 103–106.

Hesse, R., and S. Khodabakhsh (2016), Anatomy of Labrador Sea Heinrich layers, *Mar. Geol.*, *380*, 44–66, doi:10.1016/j.margeo.2016.05.019.

Hesse, R., H. Rashid, and S. Khodabakhsh (2004), Fine-grained sediment lofting from meltwater-generated turbidity currents during Heinrich events, *Geology*, *32*, 449–452.

Hiscott, R. N., A. E. Aksu (1996), Quaternary sedimentary processes and budgets in Orphan Basin, Southwestern Labrador Sea, *Quat. Res.*, *4*(2), 160–175.

Hodell, D. A., and J. H. Curtis (2008), Oxygen and carbon isotopes of detrital carbonate in North Atlantic Heinrich events, *Mar. Geol.*, *256*, 30–35, doi:10.1016/j.margeo.2008.09.010.

Hodell, D. A., J. E. T. Channell, J. H. Curtis, O. E. Romero, and U. Röhl (2008), Onset of "Hudson Strait" Heinrich events in the eastern North Atlantic at the end of the middle Pleistocene transition (~640 ka)?, *Paleoceanography*, *23*, PA4218, doi:10.1029/2008PA001591.

Hoogakker, B. A. A., H. Elderfield, G. Schmiedl, N. McCave, and R. E. M. Rickaby (2015), Glacial–interglacial changes in bottom-water oxygen content on the Portuguese margin, *Nat. Geosci.*, *8*, 40–43.

Hulbe, C. L. (1997), An ice shelf mechanism for Heinrich layer production, *Paleoceanography*, *1*(5), 711–717, doi:10.1029/97PA02014.
Hulbe, C. L., D. R. MacAyeal, G. H. Denton, J. Kleman, and T. V. Lowell (2004), Catastrophic ice shelf breakup as the source of Heinrich event icebergs, *Paleoceanography*, *19*, PA1004, doi:10.1029/2003PA000890.
Jaccard, S. L., E. D. Galbraith, A. Martinez-Garcia, and R. R. Anderson (2016), Covariation of deep Southern Ocean oxygenation and atmospheric CO_2 through the last ice age, *Nature*, *530*, 207–210.
Jonkers, L., M. Moros, M. A. Prins, T. Dokken, C. Andersson Dahl, N. Dijkstra, K. Perner, and G.-J. A. Brummer (2010), A reconstruction of sea surface warming in the northern North Atlantic during MIS 3 ice-rafting events, *Quat. Sci. Rev.*, *29*(15), 1791–1800.
Keigwin, L. D., J. Sachs, Y. Rosenthal, and E. A. Boyle (2005), The 8200 year B.P. event in the slope water system, western subpolar North Atlantic, *Paleoceanography*, *20*, PA2003, doi:10.1029/2004PA001074.
Kennett, J. P., and M. S. Srinivasan (1983), *Neogene Planktonic Foraminifera: A Phylogenetic Atlas*, Hutchinson Ross, Stroudsburg, Pa.
MacAyeal, D. R. (1993), Binge/purge oscillations of the Laurentide Ice Sheet as a cause of the North Atlantic's Heinrich events, *Paleoceanography*, *8*, 775–784, doi:10.1029/93PA02200.
Madsen, I. C., and N. V. Y. Scarlett (2008), Quantitative phase analysis, in *Powder Diffraction: Theory and Practice*, edited by R. E. Dinnabier, Royal Society of Chemistry, Cambridge.
Mangini, A., A. Eisenhauer, and P. Walter (1990), Response of manganese in the ocean to the climatic cycles in the Quaternary, *Paleoceanography*, *5*(5), 811–821, doi:10.1029/PA005i005p00811.
Mangini, A., A. Eisenhauer, and P. Walter (1991), A spike of CO_2 in the atmosphere at glacial-interglacial boundaries induced by raid deposition of manganese in the oceans, *Tellus, Ser. B*, *43*, 97–105.
Mangini, A., M. Jung, and S. Laukenmann (2001), What do we learn from peaks of uranium and of manganese in deep sea sediments?, *Mar. Geol.*, *177*, 63–78.
Manighetti, B., I. N. McCave, M. Maslin, and N. J. Shackleton (1995), Chronology for climate change: Developing age models for the Biogeochemical Ocean Flux Study cores, *Paleoceanography*, *10*(3), 513–525, doi:10.1029/94PA03062.
Marcott, S. A., et al. (2011), Ice-shelf collapse from subsurface warming as a trigger for Heinrich events, *Proc. Nat. Acad. Sci. U.S.A.*, *108*(33), 13,415–13,419.
Marcott, S. A., et al. (2014), Centennial-scale changes in the global carbon cycle during the last deglaciation, *Nature*, *514*, 616–619.
Martrat, B., P. Jimenez-Amat, R. Zahn, and J. O. Grimalt (2014), Similarities and dissimilarities between the last two deglaciations and interglaciations in the North Atlantic region, *Quat. Sci. Rev.*, *99*, 122–134.
McManus, J. F., G. C. Bond, W. S. Broecker, S. Johnsen, L. Labeyrie, and S. Higgins (1994), High-resolution climate records from the North Atlantic during the last interglacial, *Nature*, *371*, 326–329, doi:10.1038/371326a0.
McManus, J. F., R. F. Anderson, W. S. Broecker, M. Q. Fleisher, and S. M. Higgins (1998), Radiometrically determined sedimentary fluxes in the sub-polar North Atlantic during the last 140,000 years, *Earth Planet. Sci. Lett.*, *155*, 29–43.
McManus, J. F., R. Francois, J.-M. Gherardi, L. D. Keigwin, and S. Brown-Leger (2004), Collapse and rapid resumption of Atlantic meridional circulation linked to deglacial climate changes, *Nature*, *428*(6958), 834–837.
Menviel, L., M. H. England, K. J. Meissner, A. Mouchet, and J. Yu (2014), Atlantic-Pacific seesaw and its role in outgassing CO_2 during Heinrich events, *Paleoceanography*, *29*, 58–70, doi:10.1002/2013PA002542.
Naafs, B. D. A., J. Hefter, J. Grützner, and R. Stein (2013), Warming of surface waters in the midlatitude North Atlantic during Heinrich events, *Paleoceanography*, *28*, 153–163, doi:10.1029/2012PA002354.
North Greenland Project Members (2014), High-resolution record of Northern Hemisphere climate extending into the last interglacial period, *Nature*, *431*, 147–151.
Obrochta, S. P., H. Miyahara, Y. Yokoyama, and T. J. Crowley (2012), A re-examination of evidence for the North Atlantic "1500-year cycle" at Site 609, *Quat. Sci. Rev.*, *55*, 22–33.
Obrochta, S. P., T. J. Crowley, J. E. T. Channell, D. A. Hodell, P. A. Baker, A. Seki, and Y. Yokoyama (2014), Climate variability and ice-sheet dynamics during the last three glaciations, *Earth Planet. Sci. Lett.*, *406*, 198–212.
Peck, V. L., I. R. Hall, R. Zahn, H. Elderfield, F. Grousset, S. R. Hemming, and J. D. Scourse (2006), High resolution evidence for linkages between NW European ice sheet instability and Atlantic Meridional Overturning Circulation, *Earth Planet. Sci. Lett.*, *243*, 476–488.
Rashid, H., R. Hesse, and D. J. W. Piper (2003), Origin of unusually thick ice-proximal Heinrich layers H-1 to H-3 in the northwest Labrador Sea, *Earth Planet. Sci. Lett.*, *208*, 319–336.
Rashid, H., F. Saint-Ange, D. C. Barber, M. E. Smith, and N. Devalia (2012), Fine scale sediment structure and geochemical signature between eastern and western North Atlantic during Heinrich events 1 and 2, *Quat. Sci. Rev.*, *46*, 136–150.
Reimer, P. J., et al. (2013), IntCal13 and Marine13 radiocarbon age calibration curves 0–50,000 years cal BP, *Radiocarbon*, *50*(4), 1869–1887.
Rhodes, R. H., E. J. Brook, J. C. H. Chiang, T. Blunier, O. Maselli, J. R. McConnell, D. Romanini, and J. P. Severinghaus (2015), Enhanced tropical methane production in response to iceberg discharge in the North Atlantic, *Science*, *348*(6238), 1016–1019.
Rignot, E., S. Jacobs, J. Mouginot, and B. Scheuchl (2013), Ice-shelf melting around Antarctica, *Science*, *341*, 266–270.
Rodríguez-Tovar, F. J., and J. Dorador (2015), Ichnofabric characterization in cores: A method of digital image treatment, *Ann. Soc. Geol. Pol.*, *85*, 465–471.
Röhl, U., and L. J. Abrams (2000), High-resolution, downhole and non-destructive core measurements from Sites 999 and 1001 in the Caribbean Sea: Application to the late Paleocene thermal maximum, in *Proceedings of the Ocean Drilling Program*, vol. 165, edited by R. M. Leckie et al., pp. 191–203, *Sci Results*, College Station, Tex.
Ruddiman, W. F. (1977), Late Quaternary deposition of ice-rafted sand in the subpolar North Atlantic (lat 40° to 65°N), *Geol. Soc. Am. Bull.*, *88*, 1813–1827, doi:10.1130/0016-7606(1977)88<1813:LQDOIS>2.0.CO;2.
Sanchez Goñi, M. F., and S. P. Harrison (2010), Millennial-scale climate variability and vegetation changes during the last Glacial: Concepts and terminology, *Quat. Sci. Rev.*, *29*, 2823–2827.
Sarnthein, M., S. Balmer, P. M. Grootes, and M. Mudelsee (2015), Planktic and bnethic 14C reservoir ages for three ocean basins, calibrated by a suite of 14C plateaus in the glacial-to-deglacial Suigetsu atmospheric 14C record, *Radiocarbon*, *57*(1), 129–151.
Schindelin, J., I. Arganda-Carreras, and E. Frise (2012), Fiji: An open-source platform for biological-image analysis, *Nat. Methods*, *9*(7), 676–682.
Sierro, F. J., D. A. Hodell, J. Curtis, J. A. Flores, I. Reguera, E. Colmenero-Hidalgo, M. A. Barcena, J. Grimalt, and M. Canals (2005), Impact of iceberg melting during Heinrich events on Mediterranean thermohaline circulation, *Paleoceanography*, *20*, PA2019, doi:10.1029/2004PA001051.
Sigman, D., A. M. de Boer, and G. H. Haug (2007), Antarctic stratification, atmospheric water vapor, and Heinrich events: A hypothesis for Late Pleistocene deglaciations (geophysical monograph), in *Ocean Circulation: Mechanisms and Impacts Past and Future Changes of Meridional Overturning*, edited by A. Schmittner, J. C. H. Chiang, and S. Hemmings, pp. 335–349, AGU, Washington, D. C.

Skinner, L. C., C. Waelbroeck, A. E. Scrivner, and S. J. Fallon (2014), Radiocarbon evidence for alternating northern and southern sources of ventilation of the deep Atlantic carbon pool during the last deglaciation, *Proc. Nat. Acad. Sci. U.S.A.*, *111*(15), 5480–5484, doi:10.1073/pnas.1400668111.

Southon, J., A. L. Noronha, H. Cheng, R. L. Edwards, and Y. Wang (2012), A high-resolution record of atmospheric ^{14}C based on Hulu Cave speleothem H82, *Quat. Sci. Rev.*, *33*, 32–42.

Spötl, C., and T. W. Vennemann (2003), Continuous flow isotope ratio mass spectrometric analysis of carbonate minerals, *Rapid Commun. Mass Spectrom.*, *17*(9), 1004–1006.

Stern, J. V., and L. E. Lisiecki (2013), Termination 1 timing in radiocarbon dated regional benthic $\delta^{18}O$ stacks, *Paleoceanography*, *29*, 1127–1142, doi:10.1002/2014PA002700.

Stokes, C. R., and C. D. Clark (2001), Palaeo-ice streams, *Quat. Sci. Rev.*, *20*, 1437–1457.

Stoner, J. S., J. E. T. Channell, and C. Hillaire-Marcel (1996), The magnetic signature of rapidly deposited detrital layers from the deep Labrador Sea: Relationship to North Atlantic Heinrich layers, *Paleoceanography*, *11*(3), 309–325, doi:10.1029/96PA00583.

Svensson, A., et al. (2008), A 60000 year Greenland stratigraphic ice core chronology, *Clim. Past*, *4*, 47–57.

Syvitski, J. P. M. (1989), On the deposition of sediment within glacier-influenced fjords: Oceanographic controls, *Mar. Geol.*, *85*, 301–329.

Tamburini, F., S. Huon, P. Steinmann, F. E. Grousset, T. Adatte, and K. B. Follmi (2002), Dysaerobic conditions during Heinrich events 4 and 5: Evidence from phosphorus distribution in a North Atlantic deep-sea core, *Geochim. Cosmochim. Acta*, *66*(23), 4069–4083.

Thomson, J., N. C. Higgs, and T. Clayton (1995), A geochemical criterion for the recognition of Heinrich events and estimation of their depositional fluxes by the $^{230}Th_{excess}$ profiling method, *Earth Planet. Sci. Lett.*, *135*, 41–56.

Thomson, J., N. C. Higgs, and T. Clayton (1996), Diagenetic redistributions of redox-sensitive elements in northeast Atlantic glacial/interglacial transition sediments, *Earth Planet. Sci. Lett.*, *139*, 365–377.

Thomson, J., S. Nixon, C. P. Summerhayes, J. Schönfeld, R. Zahn, and P. Grootes (1999), Implications for sedimentation changes on the Iberian Margin over the last two glacial/interglacial transitions from $^{230}Th_{excess}$ systematics, *Earth Planet. Sci. Lett.*, *165*, 255–270.

Tjallingii, R., U. Röhl, M. Koelling, and T. Bickert (2007), Influence of the water content on X-ray fluorescence core-scanning measurements in soft marine sediments, *Geochem. Geophys. Geosyst.*, *8*, Q02004, doi:10.1029/2006GC001393.

Toucanne, S., S. Zaragosi, J.-F. Bourillet, V. Marieu, M. Cremer, M. Kageyama, B. Van Vliet-Lano, F. Eynaud, J.-L. Turon, and P. L. Gibbard (2010), The first estimation of Fleuve Manche palaeoriver discharge during the last deglaciation: Evidence for Fennoscandian ice sheet meltwater flow in the English Channel ca 20–18 ka ago, *Earth Planet. Sci. Lett.*, *290*, 459–473.

Toucanne, S., G. Soulet, N. Freslon, R. Silva Jacinto, B. Dennielou, S. Zaragosi, F. Eynaud, J.-F. Bourillet, and G. Bayon (2015), Millennial-scale fluctuations of the European Ice Sheet at the end of the last glacial, and their potential impact on global climate, *Quat. Sci. Rev.*, *123*, 113–133.

Treble, P. C., A. K. Schmitt, R. L. Edwards, K. D. McKeegan, and T. M. Harrison (2007), High resolution Secondary Ionisation Mass Spectrometry (SIMS) $\delta^{18}O$ analyses of Hulu Cave speleothem at the time of Heinrich Event 1, *Chem. Geol.*, *238*, 197–212.

Vautravers, M. J., and N. J. Shackleton (2006), Centennial-scale surface hydrology off Portugal during marine isotope stage 3: Insights from planktonic foraminiferal fauna variability, *Paleoceanography*, *21*, PA3004, doi:10.1029/2005PA001144.

Vautravers, M. J., N. J. Shackleton, C. Lopez-Martinez, and J. O. Grimalt (2004), Gulf Stream variability during marine isotope stage 3, *Paleoceanography*, *19*, PA2011, doi:10.1029/2003PA000966.

Wang, Y. J., H. Cheng, R. L. Edwards, Z. S. An, J. Y. Wu, C. C. Shen, and J. A. Dorale (2001), A high-resolution absolute-dated Late Pleistocene monsoon record from Hulu Cave, China, *Science*, *294*, 2345–2348.

Wolff, E. W., H. Fischer, and R. Röthlisberger (2009), Glacial terminations as southern warmings without northern control, *Nat. Geosci.*, *2*, 206–209.

Wu, J. Y., Y. J. Wang, H. Cheng, and R. L. Edwards (2009), An exceptionally strengthened East Asian summer monsoon event between 19.9 and 17.1 ka BP recorded in a Hulu stalagmite, *Sci. China, Ser. D Earth Sci.*, *52*, 360–368.

Zhang, W., W. Jiangying, Y. Wang, Y. Wang, H. Cheng, X. Kong, and F. Duan (2014), A detailed East Asian monsoon history surrounding the "Mystery Interval" derived from three Chinese speleothem records, *Quat. Res.*, *82*, 154–163.